Article

Ubiquitous acceleration in Greenland Ice Sheet calving from 1985 to 2022

https://doi.org/10.1038/s41586-023-06863-2

Received: 3 August 2023

Accepted: 9 November 2023

Published online: 17 January 2024

Check for updates

Chad A. Greene[1]✉, Alex S. Gardner[1], Michael Wood[2] & Joshua K. Cuzzone[3]

Nearly every glacier in Greenland has thinned or retreated over the past few decades[1–4], leading to glacier acceleration, increased rates of sea-level rise and climate impacts around the globe[5–9]. To understand how calving-front retreat has affected the ice-mass balance of Greenland, we combine 236,328 manually derived and AI-derived observations of glacier terminus positions collected from 1985 to 2022 and generate a 120-m-resolution mask defining the ice-sheet extent every month for nearly four decades. Here we show that, since 1985, the Greenland Ice Sheet (GrIS) has lost 5,091 ± 72 km^2 of area, corresponding to 1,034 ± 120 Gt of ice lost to retreat. Our results indicate that, by neglecting calving-front retreat, current consensus estimates of ice-sheet mass balance[4,9] have underestimated recent mass loss from Greenland by as much as 20%. The mass loss we report has had minimal direct impact on global sea level but is sufficient to affect ocean circulation and the distribution of heat energy around the globe[10–12]. On seasonal timescales, Greenland loses 193 ± 25 km^2 (63 ± 6 Gt) of ice to retreat each year from a maximum extent in May to a minimum between September and October. We find that multidecadal retreat is highly correlated with the magnitude of seasonal advance and retreat of each glacier, meaning that terminus-position variability on seasonal timescales can serve as an indicator of glacier sensitivity to longer-term climate change.

The GrIS has been a main contributor to global sea-level rise over the past century and its rate of mass loss has accelerated substantially since the 1990s[1,4,9]. Climate projections indicate with virtual certainty that Greenland will continue to lose ice mass throughout this century[9,13], but the timing, magnitude and character of future changes to the ice sheet will depend on the severity of climate forcing and the sensitivity that each glacier exhibits to changes in its environment. Observations suggest that terminus retreat may be the most reliable indicator of glacier sensitivity to climate change[3] and, although retreat is an effect of climate change, it can also cause sea-level rise, as each calving event affects the internal stress regime within the ice sheet and tends to result in glacier acceleration[5,6]. Ice-sheet models reinforce the importance of terminus retreat as a leading indicator of change, showing that sea-level projections are much higher when long-term terminus retreat is included[14], and that neglecting seasonal oscillations of terminus position produces biased projections of decadal mass change[15,16]. A complete understanding of the past behaviour, current state and future vulnerability of the GrIS therefore requires a complete picture of how and when the ice sheet has changed in areal extent on seasonal to decadal timescales.

We combine 236,328 observations of glacier terminus positions (Fig. 1) with an ice-flow model to develop a consistent, 120-m-resolution, time-evolving ice mask that captures the areal extents of the entire GrIS at monthly intervals from 1985 to 2022 (Methods). Terminus positions were compiled from several public datasets, which were derived using manual or automated means to trace the seaward edges of glaciers in optical and radar satellite images. We use a constant-velocity flow model, which allows us to identify and discard erroneous terminus-position picks, estimate the position of glacier termini in months that do not contain direct observations and ensure that glacier termini can only express plausible rates of advance. The flow model allows us to estimate terminus positions between observations by interpolation and ensures that ice fronts remain within the bounds of the most recent (past) and next (future) observations of terminus position, at any given time and location. As well as developing a dataset to quantify areal changes of the GrIS, we also estimate the ice thickness corresponding to every pixel in the time-evolving ice mask, with a goal of understanding the exact timing and magnitude of mass changes over the past few decades.

Decades of retreat

From August 1985 to February 2022, the GrIS lost 5,091 ± 72 km^2 of its area to secular glacier terminus retreat, which corresponds to 1,034 ± 120 Gt of ice loss beyond the steady-state calving rate that would be necessary to maintain constant areal extents of the ice sheet (Fig. 2 and Supplementary Table 1). The timing of retreat is characterized by relatively steady areal extents of the GrIS until the late 1990s, followed by a 218 km^2 year^{-1} (42 Gt year^{-1}) rate of loss since January 2000, without any marked slowdown in the retreat rate so far (Extended Data Fig. 1). Area (and mass) loss are observed in all regions of the ice sheet, led by 980 ± 13 km^2 (160 ± 104 Gt) from Zachariæ Isstrøm, 188 ± 3 km^2

[1]Jet Propulsion Laboratory, California Institute of Technology, Pasadena, CA, USA. [2]Moss Landing Marine Laboratories, San José State University, San José, CA, USA. [3]Joint Institute for Regional Earth System Science and Engineering, University of California, Los Angeles, Los Angeles, CA, USA. ✉e-mail: cgreene@jpl.nasa.gov

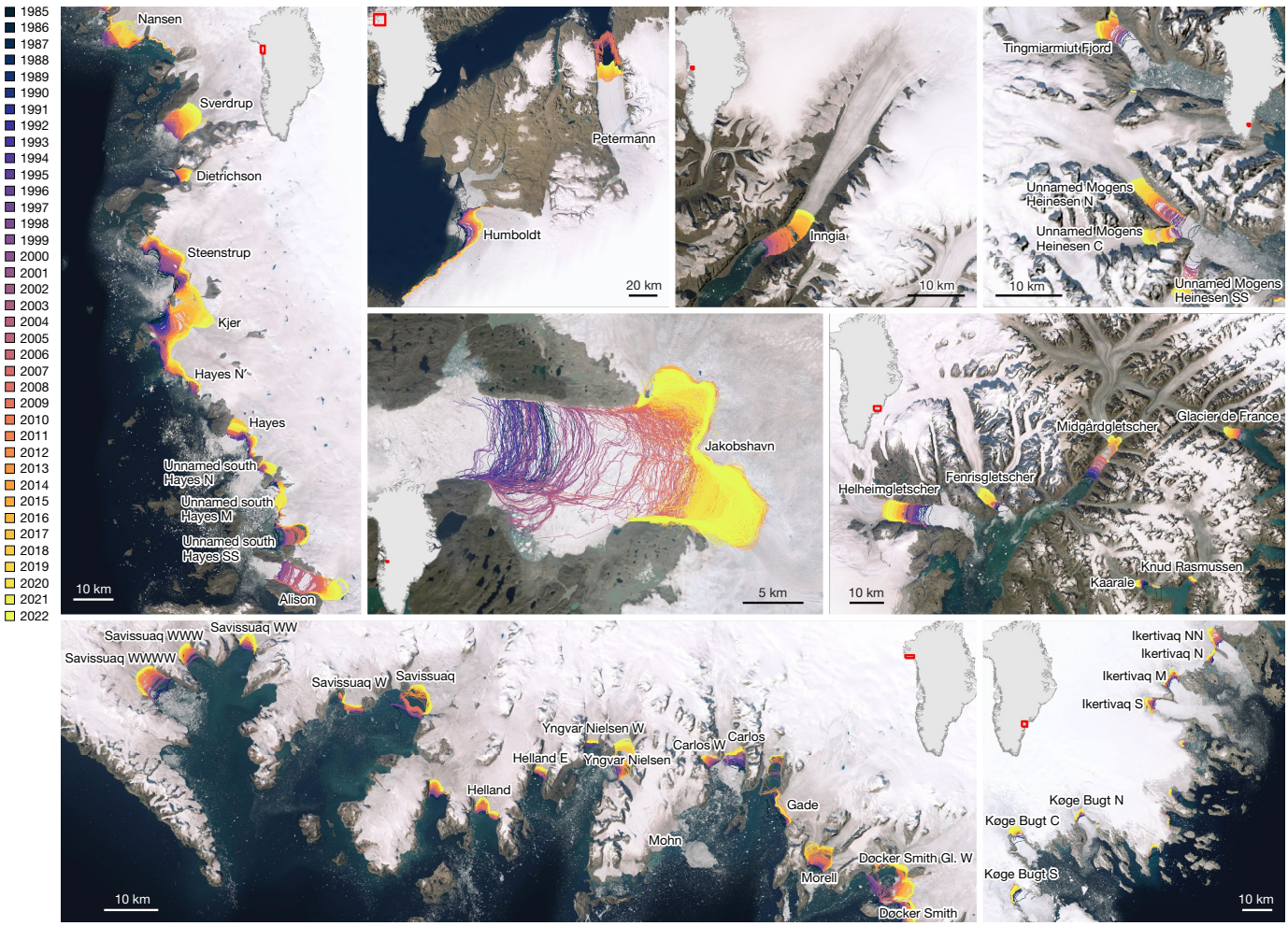

Fig. 1 | Greenland glacier terminus observations since 1985. We use 236,328 manually derived and artificial intelligence (AI)-derived glacier terminus observations from five publicly available datasets (Methods) to investigate ice-sheet retreat in recent decades. Early observations are shown as dark blue lines, which are generally seaward of the present-day edge of the ice sheet, whereas more recent observations are shown in yellow and, in some locations, have migrated more than 10 km inland since 1985. An arbitrary selection of locales from all quadrants of the Greenland coast are presented here to illustrate the diversity of geographic settings through which a common signal of terminus retreat has etched its way slowly towards the interior of the ice sheet. Maps created with Arctic Mapping Tools for MATLAB[54] and ArcGIS with basemap imagery credit to Esri, Maxar, Earthstar Geographics and the GIS user community.

(88 ± 24 Gt) from Jakobshavn Isbræ and 343 ± 18 km^2 (87 ± 3 Gt) from Humboldt Gletscher. During the study period, Nioghalvfjerdsfjorden (79° N) lost 282 ± 12 km^2 (41 ± 32 Gt), which represents a greater area loss than Jakobshavn Isbræ, but its impact on ice-sheet mass change was less substantial, owing to differences in ice thickness. We use observations from 207 glacier catchments in this study (203 marine-terminating and four land-terminating), which together represent 87% of the total GrIS area and 90% of the total mass of the ice sheet. Among all of the glacier catchments we observe, we find that only Qajuuttap Sermia exhibited gains beyond measurement uncertainty, and its increase of 1.4 ± 0.6 km^2 (0.4 ± 0.3 Gt) is rather small in comparison with losses observed elsewhere around the ice sheet.

Greenland's great 'winter perennials'

On seasonal timescales, we confirm a well-documented pattern of glacier growth throughout winter towards a maximum extent in late spring, followed by calving and retreat throughout the summer, then reaching a minimum extent in the autumn[7,8,17,18]. Year-round observations have been abundant since the 2014 launch of the Sentinel-1A radar imaging satellite (Extended Data Fig. 2), so we use 2014–2020 as the most well-constrained years to characterize seasonal cycles of growth and retreat. We subtract a 12-month moving mean from pan-GrIS totals and take the monthly median of the subannual residuals, to find that the ice sheet reaches a maximum extent each May, then loses 193 ± 25 km^2 (63 ± 6 Gt) to reach a minimum extent in September or October (Extended Data Fig. 1). Among the glaciers we survey, 87% exhibit variability in areal extent exceeding measurement uncertainty and the timing of seasonal growth and retreat is relatively uniform across the entire ice sheet (Fig. 3). The largest seasonal signal by far is observed at Jakobshavn Isbræ, which grows and shrinks by 18.6 ± 3.8 km^2 (13.6 ± 2.6 Gt) each year and has a notable distinction of reaching its maximum and minimum extents in April and August, a full month or more before the GrIS as a whole. The seasonal cycle of Zachariæ Isstrøm is inconsistent from year to year owing to the complex and evolving geometry of its retreating ice front, but the ice stream averages 15.3 ± 5.6 km^2 (7.5 ± 2.5 Gt) net ablation each summer. Meanwhile, the thicker ice of the fjord-bound Kangerlussuaq exhibits an average summer retreat of 9.5 ± 5.2 km^2 (7.0 ± 3.4 Gt). We do not detect seasonal area variability in any of the four land-terminating glaciers we observe, reflecting a common role that the ocean plays in driving the advance and retreat of Greenland's glaciers on seasonal timescales.

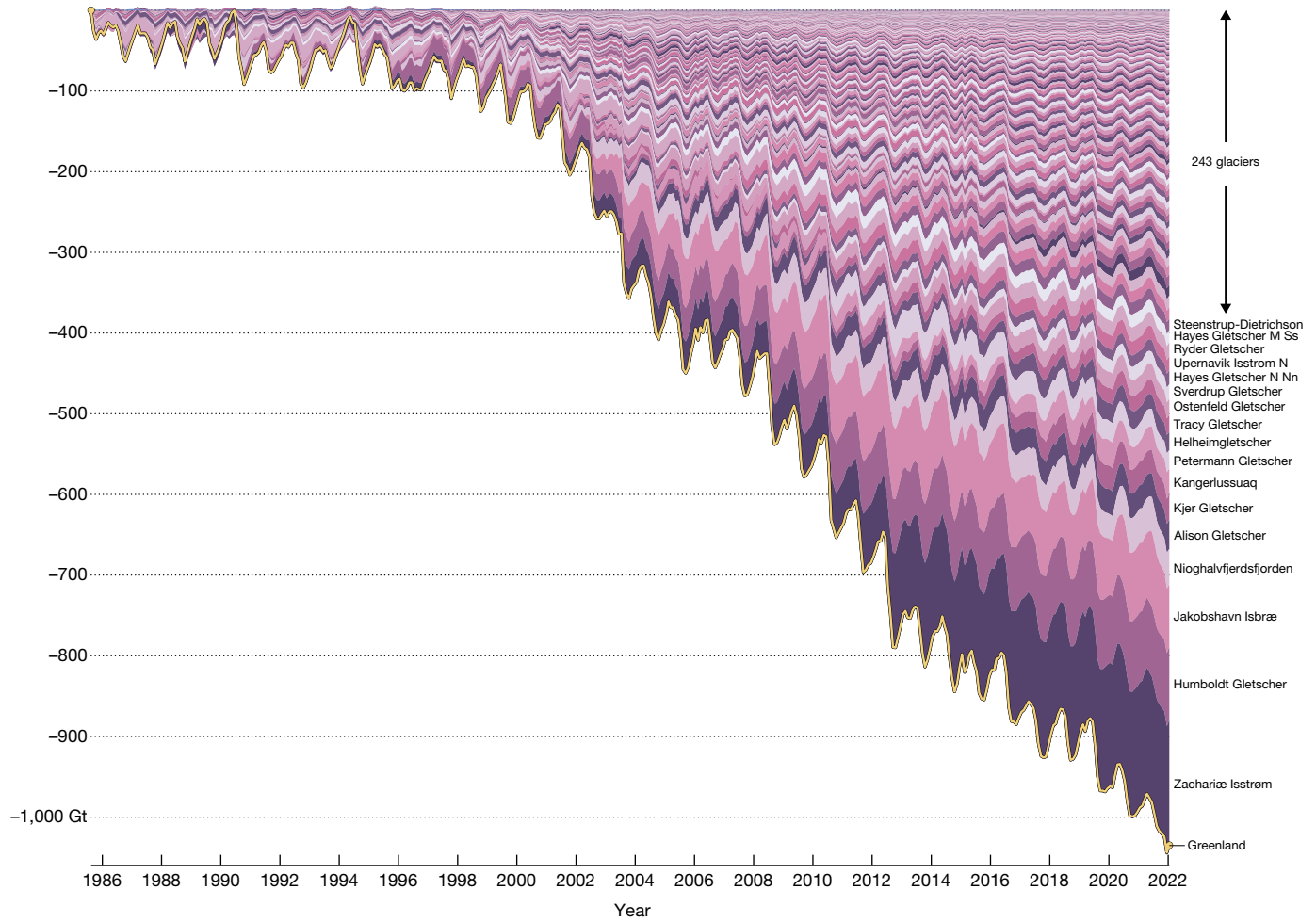

Fig. 2 | Cumulative mass change resulting from glacier retreat since 1985. Almost every glacier in Greenland has lost substantial mass since 1985. This stacked-area time series depicts the mass change of each glacier, sorted with the greatest losses at the bottom. Losses from all glaciers in this study total 1,034 ± 120 Gt, led by Zachariæ Isstrøm, Humboldt Gletscher and Jakobshavn Isbræ.

Our observations of land-terminating glaciers are limited, but among the 203 marine-terminating glaciers observed in this study, 178 exhibit seasonal variability in area and mass that exceeds the uncertainty in our measurements, with relatively consistent timing and magnitude each year (Extended Data Fig. 3).

Patterns in the data

A comparison of the range of seasonal variability to the corresponding mass loss of each glacier since 1985 reveals a striking pattern (Fig. 3): glaciers that exhibit the greatest advance and retreat on seasonal timescales have generally retreated more than any others since 1985. Jakobshavn Isbræ and Zachariæ Isstrøm are characterized by the largest seasonal signals in Greenland, and these two glaciers have lost more mass than any others to secular retreat over the past several decades. Seven of the eight glaciers with the largest seasonal mass variability in Greenland are among the eight glaciers that have lost the most mass to long-term retreat since 1985.

To understand the environmental factors that may predispose a glacier to long-term mass loss, we seek relationships between the catchment-scale mass changes we have observed since 1985 and several variables that could potentially act as predictors of long-term mass change. Specifically, we consider the importance of glacier bed slope, surface slope, bed elevation at the terminus, terminus thickness, terminus width, terminus velocity, ice flux at the terminus, climatological mean surface runoff, oceanographic sill depth and mean oceanographic temperature in the waters near each glacier terminus measured from 2015 to 2022 (Methods). Among these simple potential predictors of long-term retreat, the range of seasonal mass variability stands out as the most highly correlated with the mass loss observed over the past few decades ($r^2 = 0.71$), followed by the flux ($r^2 = 0.55$), width ($r^2 = 0.44$), thickness ($r^2 = 0.36$) and bed elevation ($r^2 = 0.34$) at the terminus of each glacier (Fig. 4). Some of the largest mass signals occur where ice is thick or wide, so we normalize by the area of each glacier terminus face, finding that seasonal variability is the only notable predictor of long-term change among the candidates we investigate (Extended Data Fig. 4). We find very little correlation between decadal retreat and timing of seasonal maximum, mean rates of surface runoff, bed slope, surface slope, ice velocity at the terminus, oceanographic sill depth or the observed temperature of nearby waters.

It is perhaps unsurprising that the mass loss associated with glacier terminus retreat since 1985 is highly correlated with the range of mass variability on seasonal timescales, because the largest glaciers are most capable of producing the largest mass signals on any timescale. However, none of the glaciers exhibiting large seasonal mass variability have shown large signals of mass gain over recent decades. After normalizing mass changes by glacier terminus face area to analyse signals of effective glacier length, seasonal length variability remains the best predictor of glacier length change over decadal timescales (Extended Data Fig. 4). It is clear that a widespread forcing mechanism

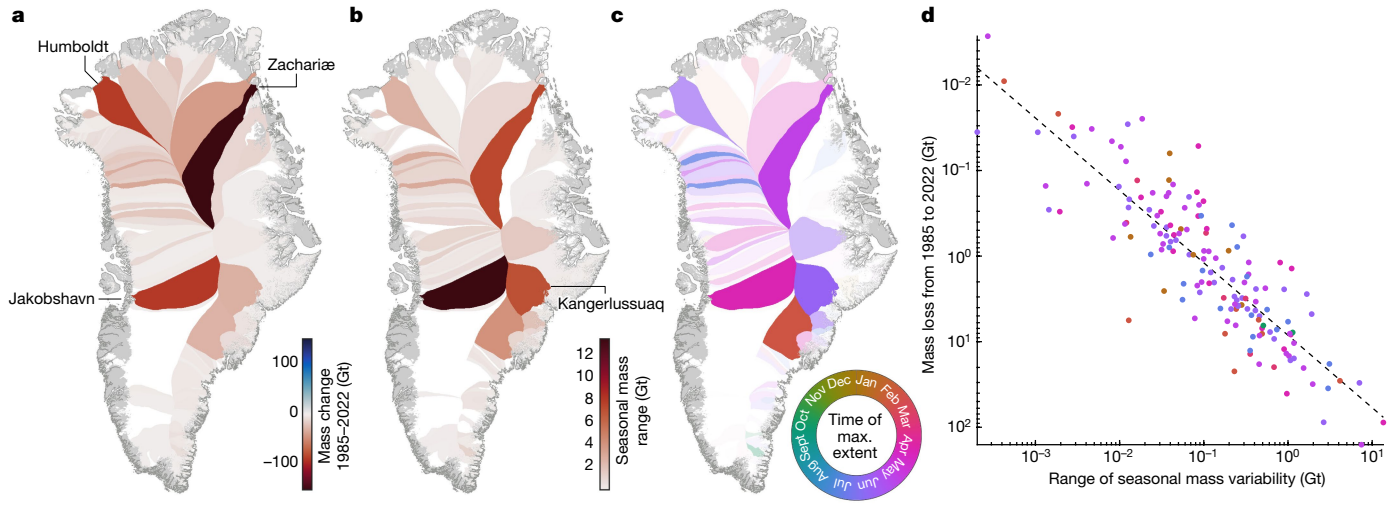

Fig. 3 | Relationship between seasonality and decadal retreat. In Greenland, the glaciers that have retreated the most over the past few decades are also characterized by notable advance and retreat cycles that occur seasonally. **a**, Net mass change owing to calving-front advance or retreat within each ice catchment since 1985. Ice-free areas are shown in grey. **b**, The median range of seasonal ice-mass variability within each glacier catchment. **c**, Month of climatological maximum extent each year. Most glaciers reach a maximum in May or June and then begin a summer-long period of retreat. The seasonal cycle of Jakobshavn Isbræ occurs at least a month earlier than most other glaciers, with its maximum extent typically observed in April. **d**, The net mass loss of each glacier catchment since 1985 is plotted as a function of its range of seasonal variability, with the dashed line indicating a linear least-squares fit to the log of mass values for each catchment. Maps created with Arctic Mapping Tools for MATLAB[54] using geographic outlines developed in this work.

has touched nearly every glacier in Greenland over the past few decades and has most considerably affected the glaciers that show sensitivity to environmental change on seasonal timescales. We expect that continued warming will produce the greatest impact on these same glaciers.

We consider several glacier characteristics that could be linked to long-term retreat. Bed slope is a fundamental characteristic of any glacier system and can throttle ice flow[19] or allow for rapid runaway retreat[20]. Likewise, surface slope is the sole driving mechanism that creates glacier flow, yet neither of these simple geometric characteristics shows a clear relationship with retreat among the glaciers we study. Surface runoff has been found to drive velocity variability on seasonal timescales[21] and has been linked to terminus advance and retreat in some localized studies[22], but—across Greenland—we find little correlation between mean runoff and long-term retreat or seasonal variability in terminus position. Terminus thickness, width, bed elevation and catchment flux are all related to the area of a glacier face and are correlated with mass signals on seasonal to decadal timescales, but when mass signals are normalized by terminus face area, we find no strong correlations between terminus geometry and effective length variability on any timescale (Extended Data Fig. 4).

Glacier response to summer warming

The environment that surrounds glaciers in Greenland undergoes considerable variation on seasonal timescales. Summer ocean warming and influxes of meltwater runoff elevate melt rates[22,23] and can alter the thickness and tensile strength of glacial ice. By winter, fjords fill with a melange of sea ice and icebergs that can exert a backstress and further modify the tensile stress within the ice near glacier termini. Calving rates respond roughly proportionally to changes in the tensile stress at the terminus of a glacier[24], so the processes that influence tensile stress on seasonal timescales offer a window into the impacts of longer-term change. The amount of warming that Greenland experiences each year from winter to summer is far greater than the total rise in annual average temperatures over the past several decades, meaning that the seasonal variability in glacier tensile stress is probably much larger than any environmentally induced secular trend. Thus, if a glacier is insensitive to large seasonal changes in tensile stress, it is probably insensitive to environmentally induced secular trends and vice versa. A notable caveat to this theory is that the predictive relationship only holds true if there is no substantial change in terminus stress regime. For instance, in the extreme case that a terminus retreats from a bathymetric rise or 'pinning point', it will instantly change from a compressional regime to a tensile regime and rates of calving will respond accordingly, independent of its previous sensitivity to changes in seasonal forcing.

Every glacier that has retreated appreciably since 1985 comes in direct contact with the ocean at its terminus and warm ocean water is undoubtedly responsible for driving much of the decadal retreat that we report[2]. We compute ocean profile temperature anomalies from observations collected by NASA's Oceans Melting Greenland project (Methods; Extended Data Fig. 5) and analyse the mean of all anomalies within 10 km of each glacier terminus, but find no clear connection between local ocean temperature and decadal retreat. The local thermal anomalies we consider are clearly regional, with the warmest temperatures in the south and the coldest temperatures in the north, whereas the glacier retreat we observe is apparent in all sectors of the ice sheet. We also investigate the role of fjord sill depth as a proxy for connection to the open ocean (Methods), but our analysis finds no link between this simple metric and the sensitivity of glaciers on seasonal or decadal timescales. We note that, although we find no link between the spatial distribution of mean ocean temperatures and the spatial distribution of glacier retreat, our analysis is independent of temporal changes in ocean temperature and we expect that glaciers will continue to retreat in response to continued ocean warming.

Impacts of mass loss

We report a widespread glacier terminus retreat in Greenland that has resulted in more than 1,000 Gt of ice loss that has not been accounted for in current observation-based estimates of ice-sheet mass balance. The terminus retreat we describe has not been captured in altimetry-based estimates, which have historically used fixed ice masks and tend to perform poorly near ice edges[25,26]. Similarly, an 'input–output' technique[1,27] offers an independent method of estimating ice-sheet mass balance by measuring surface velocity but relies on fixed flux gates that cannot capture the retreat that we report. By our estimates, almost 90% of the

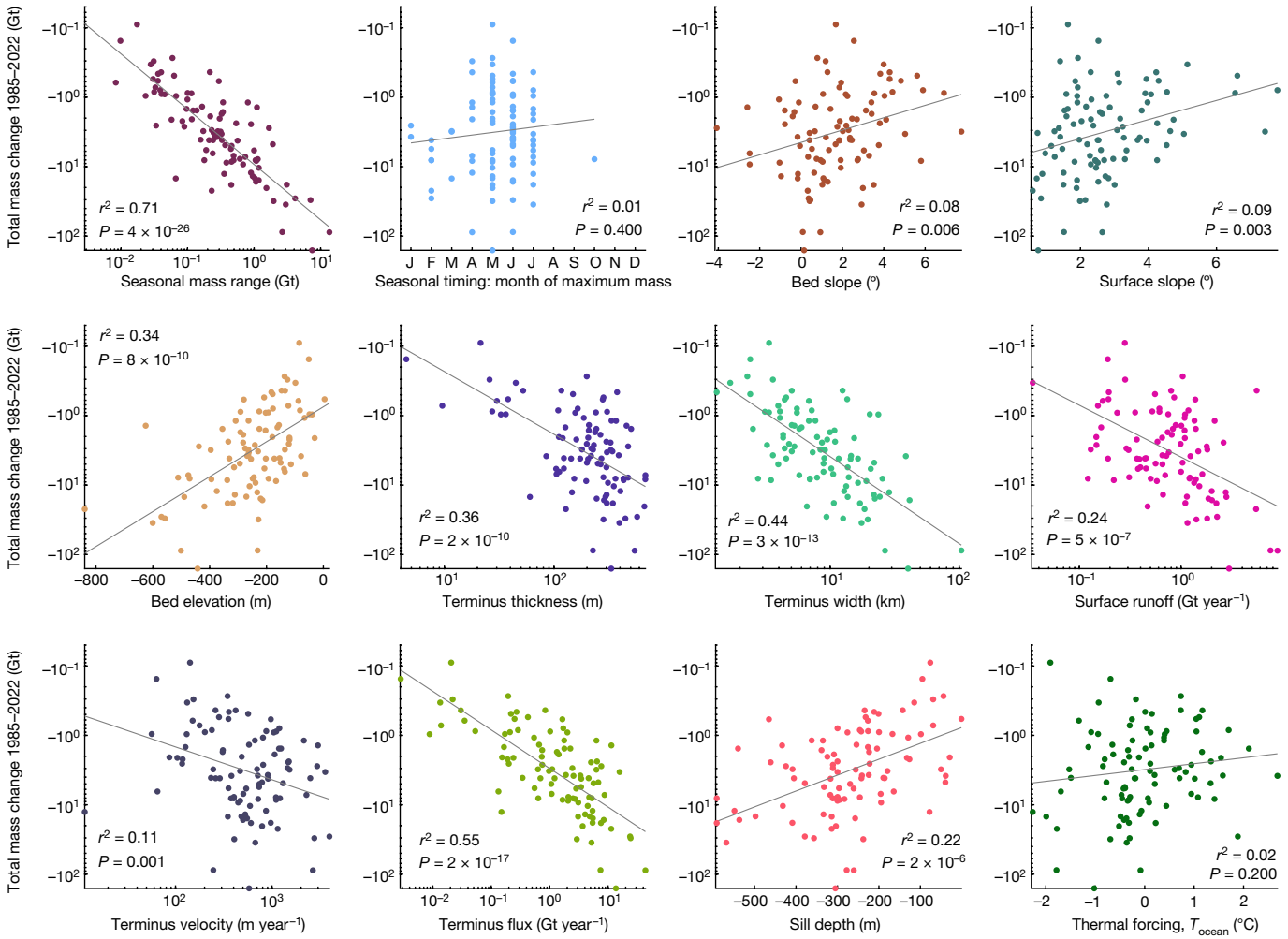

Fig. 4 | Predictors of glacier sensitivity. Decadal mass loss from calving of 95 Greenlandic glaciers is plotted as a function of 12 candidate predictors of sensitivity to climate change. The strongest correlation is seen with the range of advance and retreat that each glacier exhibits on seasonal timescales. Some correlation is apparent with glacier thickness, width, bed elevation and annual ice flux, which is to be expected, as thicker, wider glaciers are more likely to exhibit larger mass variability. After normalizing by the area of each glacier terminus face, seasonal variability is the only notable predictor of longer-term retreat (Extended Data Fig. 4). Comparisons are presented for 95 glaciers for which observations of all variables are available.

ice loss we report occurred below the surface of hydrostatic equilibrium and has since been replaced by seawater and, thus, cannot be detected by satellite gravimetry (and does not directly contribute to sea-level change beyond thermosteric effects). The remaining 120 Gt (about 0.33 mm global sea-level equivalent) of ice lost from above the surface of hydrostatic equilibrium is theoretically detectable by gravimetry, but the areas of loss are too small in spatial scale for their locations to be pinpointed by GRACE[28].

None of the three most commonly used methods of measuring ice-sheet mass balance are designed to measure the mass loss we report, meaning that the GrIS has probably lost 20% more ice since 1985 than has recently been reported[1,4,25–27,29,30]. The most recent update to the Ice sheet Mass Balance Inter-comparison Exercise (IMBIE) provides a reconciled estimate of 27 independent observation-based estimates of ice-sheet mass balance, finding an overall loss rate of 221 Gt year^{-1} between 2003 and 2018. We find that, over the same period, terminus retreat caused a further 43 Gt year^{-1} of ice loss that was not captured by any of the three geodetic techniques used in the IMBIE consensus, has not been accounted for in any large study of GrIS mass balance and represents a source of solid freshwater flux that has not been included in previous budgets of discharge to the ocean[31].

The addition of more than 1,000 Gt of freshwater to the North Atlantic Ocean since 1985 provides a buoyancy force that could strengthen the coastal currents of Greenland[32,33], change the course of future ice–ocean interactions[34,35] and weaken the Atlantic Meridional Overturning Circulation (AMOC)[36–38]. The out-of-balance anomalies we report are modest in comparison with the approximately 500 Gt of ice that flows from the GrIS each year[1,27], but there is some concern that any small source of freshwater may serve as a 'tipping point'[39] that could trigger a full-scale collapse of the AMOC[40,41], disrupting global weather patterns[42,43], ecosystems[44,45] and global food security[46,47]; yet, freshwater from the glacier retreat of Greenland is not included in oceanographic models[48,49] or estimates of state[50] at present. The energy required to melt more than 1,000 Gt of ice is notable (>3,340 exajoules), yet this heat sink is not accounted for in the present Earth energy budgets that are essential for understanding the full scope of global warming[51]. With the decades-long record of monthly ice masks we provide for the GrIS, freshwater representation in ocean models and Earth energy budgets may be improved. Likewise, the time-evolving ice masks we provide will allow improved representation of the stress state of the entire GrIS in ice-sheet models, including full representation of the seasonal cycles that are known to bias long-term estimates of sea-level rise when neglected[16]. Underestimates of mass loss in historical model reconstructions have, in fact, cast doubt on future projections of sea-level rise[52], but the time-evolving ice masks we provide will allow for improved transient calibrations, which can decrease model error[53].

Retreating in formation

The observations we present reveal an ice sheet whose areal extent varies on seasonal to decadal timescales. Despite residing in a great diversity of catchment sizes, bed configurations and geographic settings, the glaciers of Greenland march in synchronicity—growing slowly over winter, reaching a maximum extent in spring, retreating throughout the summer and starting the cycle again each autumn. Nearly every glacier in Greenland has retreated over the past few decades and, in a warming world, we posit that the glaciers that are most sensitive to changes on seasonal timescales will show the greatest sensitivity to future climate change.

Online content

Any methods, additional references, Nature Portfolio reporting summaries, source data, extended data, supplementary information, acknowledgements, peer review information; details of author contributions and competing interests; and statements of data and code availability are available at https://doi.org/10.1038/s41586-023-06863-2.

1. Mouginot, J. et al. Forty-six years of Greenland Ice Sheet mass balance from 1972 to 2018. *Proc. Natl Acad. Sci.* **116**, 9239–9244 (2019).
2. Wood, M. et al. Ocean forcing drives glacier retreat in Greenland. *Sci. Adv.* **7**, eaba7282 (2021).
3. Moon, T. A., Gardner, A. S., Csatho, B., Parmuzin, I. & Fahnestock, M. A. Rapid reconfiguration of the Greenland Ice Sheet coastal margin. *J. Geophys. Res. Earth Surf.* **125**, e2020JF005585 (2020).
4. Otosaka, I. N. et al. Mass balance of the Greenland and Antarctic ice sheets from 1992 to 2020. *Earth Syst. Sci. Data* **15**, 1597–1616 (2023).
5. Nick, F. M., Vieli, A., Howat, I. M. & Joughin, I. Large-scale changes in Greenland outlet glacier dynamics triggered at the terminus. *Nat. Geosci.* **2**, 110–114 (2009).
6. King, M. D. et al. Dynamic ice loss from the Greenland Ice Sheet driven by sustained glacier retreat. *Commun. Earth Environ.* **1**, 1 (2020).
7. Moon, T., Joughin, I. & Smith, B. Seasonal to multiyear variability of glacier surface velocity, terminus position, and sea ice/ice mélange in northwest Greenland. *J. Geophys. Res. Earth Surf.* **120**, 818–833 (2015).
8. Vijay, S. et al. Resolving seasonal ice velocity of 45 Greenlandic glaciers with very high temporal details. *Geophys. Res. Lett.* **46**, 1485–1495 (2019).
9. Fox-Kemper, B. et al. in *Climate Change 2021: The Physical Science Basis. Contribution of Working Group I to the Sixth Assessment Report of the Intergovernmental Panel on Climate Change* (eds Masson-Delmotte, V. et al.) 1211–1362 (Cambridge Univ. Press, 2021).
10. Enderlin, E. M., Hamilto, G. S., Straneo, F. & Sutherland, D. A. Iceberg meltwater fluxes dominate the freshwater budget in Greenland's iceberg-congested glacial fjords. *Geophys. Res. Lett.* **43**, 11,287–11,294 (2016).
11. Marsh, R. et al. Short-term impacts of enhanced Greenland freshwater fluxes in an eddy-permitting ocean model. *Ocean Sci.* **6**, 749–760 (2010).
12. Böning, C. W., Behrens, E., Biastoch, A., Getzlaff, K. & Bamber, J. L. Emerging impact of Greenland meltwater on deepwater formation in the North Atlantic Ocean. *Nat. Geosci.* **9**, 523–527 (2016).
13. Choi, Y., Morlighem, M., Rignot, E. & Wood, M. Ice dynamics will remain a primary driver of Greenland ice sheet mass loss over the next century. *Commun. Earth Environ.* **2**, 26 (2021).
14. Rückamp, M., Goelzer, H. & Humbert, A. Sensitivity of Greenland ice sheet projections to spatial resolution in higher-order simulations: the Alfred Wegener Institute (AWI) contribution to ISMIP6 Greenland using the Ice-sheet and Sea-level System Model (ISSM). *Cryosphere* **14**, 3309–3327 (2020).
15. Robel, A. A., Roe, G. H. & Haseloff, M. Response of marine-terminating glaciers to forcing: time scales, sensitivities, instabilities, and stochastic dynamics. *J. Geophys. Res. Earth Surf.* **123**, 2205–2227 (2018).
16. Felikson, D., Nowicki, S., Nias, I., Morlighem, M. & Seroussi, H. Seasonal tidewater glacier terminus oscillations bias multi-decadal projections of ice mass change. *J. Geophys. Res. Earth Surf.* **127**, e2021JF006249 (2022).
17. Schild, K. M. & Hamilton, G. S. Seasonal variations of outlet glacier terminus position in Greenland. *J. Glaciol.* **59**, 759–770 (2013).
18. Black, T. E. & Joughin, I. Weekly to monthly terminus variability of Greenland's marine-terminating outlet glaciers. *Cryosphere* **17**, 1–13 (2023).
19. Felikson, D. et al. Steep glacier bed knickpoints mitigate inland thinning in Greenland. *Geophys. Res. Lett.* **48**, e2020GL090112 (2021).
20. Schoof, C. Ice sheet grounding line dynamics: steady states, stability, and hysteresis. *J. Geophys. Res. Earth Surf.* **112**, F03S28 (2007).
21. Ultee, L., Felikson, D., Minchew, B., Stearns, L. A. & Riel, B. Helheim Glacier ice velocity variability responds to runoff and terminus position change at different timescales. *Nat. Commun.* **13**, 6022 (2022).
22. Fried, M. J. et al. Reconciling drivers of seasonal terminus advance and retreat at 13 Central West Greenland tidewater glaciers. *J. Geophys. Res. Earth Surf.* **123**, 1590–1607 (2018).
23. Xu, Y., Rignot, E., Menemenlis, D. & Koppes, M. Numerical experiments on subaqueous melting of Greenland tidewater glaciers in response to ocean warming and enhanced subglacial discharge. *Ann. Glaciol.* **53**, 229–234 (2012).
24. Morlighem, M., Wood, M., Seroussi, H., Choi, Y. & Rignot, E. Modeling the response of northwest Greenland to enhanced ocean thermal forcing and subglacial discharge. *Cryosphere* **13**, 723–734 (2019).
25. Simonsen, S. B., Barletta, V. R., Colgan, W. T. & Sørensen, L. S. Greenland Ice Sheet mass balance (1992–2020) from calibrated radar altimetry. *Geophys. Res. Lett.* **48**, e2020GL091216 (2021).
26. Smith, B. et al. Pervasive ice sheet mass loss reflects competing ocean and atmosphere processes. *Science* **368**, 1239–1242 (2020).
27. Mankoff, K. D. et al. Greenland ice sheet mass balance from 1840 through next week. *Earth Syst. Sci. Data* **13**, 5001–5025 (2021).
28. Velicogna, I. & Wahr, J. Time-variable gravity observations of ice sheet mass balance: precision and limitations of the GRACE satellite data. *Geophys. Res. Lett.* **40**, 3055–3063 (2013).
29. The IMBIE Team. Mass balance of the Greenland Ice Sheet from 1992 to 2018. *Nature* **579**, 233–239 (2020).
30. Khan, S. A. et al. Greenland mass trends from airborne and satellite altimetry during 2011–2020. *J. Geophys. Res. Earth Surf.* **127**, e2021JF006505 (2022).
31. Bamber, J. L. et al. Land ice freshwater budget of the Arctic and North Atlantic Oceans: 1. Data, methods, and results. *J. Geophys. Res. Oceans* **123**, 1827–1837 (2018).
32. Sutherland, D. A. & Pickart, R. S. The East Greenland coastal current: structure, variability, and forcing. *Prog. Oceanogr.* **78**, 58–77 (2008).
33. Gou, R., Pennelly, C. & Myers, P. G. The changing behavior of the West Greenland current system in a very high-resolution model. *J. Geophys. Res. Oceans* **127**, e2022JC018404 (2022).
34. Davison, B. J., Cowton, T. R., Cottier, F. R. & Sole, A. J. Iceberg melting substantially modifies oceanic heat flux towards a major Greenlandic tidewater glacier. *Nat. Commun.* **11**, 5983 (2020).
35. Castro De La Guardia, L., Hu, X. & Myers, P. G. Potential positive feedback between Greenland Ice Sheet melt and Baffin Bay heat content on the west Greenland shelf. *Geophys. Res. Lett.* **42**, 4922–4930 (2015).
36. Rahmstorf, S. et al. Exceptional twentieth-century slowdown in Atlantic Ocean overturning circulation. *Nat. Clim. Change* **5**, 475–480 (2015).
37. Swingedouw, D. et al. AMOC recent and future trends: a crucial role for oceanic resolution and Greenland melting? *Front. Clim.* **4**, 838310 (2022).
38. Bakker, P. et al. Fate of the Atlantic Meridional Overturning Circulation: strong decline under continued warming and Greenland melting. *Geophys. Res. Lett.* **43**, 12,252–12,260 (2016).
39. Lenton, T. M. et al. Tipping elements in the Earth's climate system. *Proc. Natl Acad. Sci.* **105**, 1786–1793 (2008).
40. Liu, W., Xie, S.-P., Liu, Z. & Zhu, J. Overlooked possibility of a collapsed Atlantic Meridional Overturning Circulation in warming climate. *Sci. Adv.* **3**, e1601666 (2017).
41. Ditlevsen, P. & Ditlevsen, S. Warning of a forthcoming collapse of the Atlantic meridional overturning circulation. *Nat. Commun.* **14**, 4254 (2023).
42. Hansen, J. et al. Ice melt, sea level rise and superstorms: evidence from paleoclimate data, climate modeling, and modern observations that 2 °C global warming could be dangerous. *Atmos. Chem. Phys.* **16**, 3761–3812 (2016).
43. Ciemer, C., Winkelmann, R., Kurths, J. & Boers, N. Impact of an AMOC weakening on the stability of the southern Amazon rainforest. *Eur. Phys. J. Spec. Top.* **230**, 3065–3073 (2021).
44. Velasco, J. A. et al. Synergistic impacts of global warming and thermohaline circulation collapse on amphibians. *Commun. Biol.* **4**, 141 (2021).
45. Osman, M. B. et al. Industrial-era decline in subarctic Atlantic productivity. *Nature* **569**, 551–555 (2019).
46. Ritchie, P. D. L. et al. Shifts in national land use and food production in Great Britain after a climate tipping point. *Nat. Food* **1**, 76–83 (2020).
47. Defrance, D. et al. Consequences of rapid ice sheet melting on the Sahelian population vulnerability. *Proc. Natl Acad. Sci.* **114**, 6533–6538 (2017).
48. Lique, C., Holland, M. M., Dibike, Y. B., Lawrence, D. M. & Screen, J. A. Modeling the Arctic freshwater system and its integration in the global system: lessons learned and future challenges. *J. Geophys. Res. Biogeosci.* **121**, 540–566 (2016).
49. Fox-Kemper, B. et al. Challenges and prospects in ocean circulation models. *Front. Mar. Sci.* **6**, 65 (2019).
50. Forget, G. et al. ECCO version 4: an integrated framework for non-linear inverse modeling and global ocean state estimation. *Geosci. Model Dev.* **8**, 3071–3104 (2015).
51. von Schuckmann, K. et al. Heat stored in the Earth system: where does the energy go? *Earth Syst. Sci. Data* **12**, 2013–2041 (2020).
52. Aschwanden, A., Bartholomaus, T. C., Brinkerhoff, D. J. & Truffer, M. Brief communication: A roadmap towards credible projections of ice sheet contribution to sea level. *Cryosphere* **15**, 5705–5715 (2021).
53. Goldberg, D. N., Heimbach, P., Joughin, I. & Smith, B. Committed retreat of Smith, Pope, and Kohler Glaciers over the next 30 years inferred by transient model calibration. *Cryosphere* **9**, 2429–2446 (2015).
54. Greene, C. A., Gwyther, D. E. & Blankenship, D. D. Antarctic mapping tools for MATLAB. *Comput. Geosci.* **104**, 151–157 (2017).

Methods

To obtain a consistent, monthly ice mask that spans the entire GrIS for the past several decades, without gaps in space or time, we combine several sources of terminus-position observations with a simple ice-flow model such that erroneous terminus positions are eliminated and terminus advance is limited to physically plausible rates in months without direct observations.

Terminus-position data

We use 237,556 manually derived and AI-derived glacier terminus picks from 1972 to 2022, obtained from the sources described below. We focus our analysis primarily on the years since 1985, during which time 236,328 terminus picks were acquired. Although data coverage is generally poor before 1985, we include all available observations to help constrain the state of the ice sheet at the beginning of our analysis period. Extended Data Fig. 6 shows the temporal distribution of the acquisition times of all terminus picks, which were selected from the following datasets:

- AutoTerm: we use 153,281 terminus positions from the AutoTerm dataset[55,56], including 153,250 positions acquired since 1985. AutoTerm provides data from several optical and radar satellite sensors, spanning nearly four decades and includes winter data in recent years. Through visual inspection, we found that AutoTerm performs particularly well at some of the 295 glaciers it covers; however, data quality clearly suffers at other glaciers. Terminus-position accuracy is often dependent on satellite sensor and corresponds reasonably well with error estimates that are provided with the AutoTerm data. For our purposes, we inspected all AutoTerm picks visually to manually determine separate error thresholds for each of the 295 glaciers, such that we eliminate all data corresponding to error values that are associated with obvious outliers or asynchronous behaviour. For this reason, we use only 153,281 of the 278,239 terminus positions available in the full AutoTerm dataset.
- MEaSUREs weekly to monthly: we use the 21,990 weekly to monthly terminus positions[18,57] collected using the Sentinel-1 synthetic aperture radar since January 2015. Although the full dataset contains 23,676 terminus positions, we only use positions whose quality flag is 0.
- MEaSUREs Annual v2: we use 3,437 terminus positions from the MEaSUREs v2 dataset[58], including 2,987 picks acquired since 1985. We only use the highest-confidence data, with quality flags 0 or 2. Quality flags 1 and 3 correspond to uncertain picks or Landsat-7 SLC-off images and are not used in our study. We also eliminate redundant data by discarding any positions obtained from the same images used in MEaSUREs weekly to monthly data.
- CALFIN: we use 19,835 terminus positions from the CALFIN dataset[59,60], including 19,665 picks acquired since 1985. In this subset, we have discarded any CALFIN picks in which MEaSUREs Annual v2 manual picks are available for the same satellite image.
- TermPicks: we use 39,013 terminus positions from the TermPicks dataset[61,62], including 38,436 picks acquired since 1985. We discard any TermPicks data in which MEaSUREs Annual v2 manual picks are available for the same satellite image.

We note that the AutoTerm dataset includes a large amount of Landsat imagery that is also included in the MEaSUREs Annual v2, CALFIN and TermPicks datasets, meaning that there is some redundancy and probably some discrepancies between the various methods of terminus-position picking. We find that AutoTerm provides the most comprehensive record overall, but the width of fjord walls tend to be defined more narrowly in AutoTerm than in other datasets, meaning that the full widths of glaciers are sometimes not captured in AutoTerm. Also, in some cases, the bounding boxes of the AutoTerm picks seem to cut off the full extents of calving-front migration.

Ice-flow model. Our method of limiting terminus advance rates to physically plausible values requires knowledge of ice velocity wherever terminus positions have been active over the observation period. For a gridded velocity field, we compute the error-weighted average of the MEaSUREs ITS_LIVE velocity mosaics[63,64] and MEaSUREs Greenland Annual Ice Sheet Velocity Mosaics from SAR and Landsat[65]. Any holes in the resulting mosaic are then filled by interpolation with the MATLAB regionfill algorithm if they are surrounded on all sides by observed velocities.

Our interest in describing terminus evolution that occurred decades ago presents a challenge in which substantial retreat has occurred and modern velocity observations do not capture the previous extents of the ice sheet. We therefore use constant values of ice speed taken from the perimeter of available ice-sheet observations and extrapolate them downstream along flowlines from a palaeo-ice-sheet model. The three-dimensional, thermomechanical Ice-sheet and Sea-level System Model[66] is used following initialization procedures used in previous studies[67–69] to simulate the behaviour of the GrIS over the last deglaciation and up through the contemporary period. The model domain extends outward to the coastline, outboard of the present-day ice margin to simulate the ice-margin migration that occurred during the last deglaciation and Holocene. Horizontal mesh resolution varies from 20-km resolution in areas in which gradients in the bedrock topography are smooth to 2-km resolution in areas in which bedrock relief is high. This model was a contributing member to the most recent Ice Sheet Model Intercomparison Project 6 (ISMIP6)[70] and has been shown to capture the historical (1850–2012) mass variability in Greenland with good fidelity, as well as providing a good match to geologic indicators of past ice-margin change across the Holocene[67]. The model uses a higher-order ice-flow approximation[71], which is extruded to five layers and uses higher-order vertical finite elements[72] to compute the ice-sheet thermal evolution. Flow directions are taken from the most recent modelled time steps available for any given grid cell. The resulting velocity field is able to follow sinuous fjord geometries and the scalar values of ice speed match the speeds that have recently been observed near glacier termini. By our method, 99.9% of ice-covered grid cells use observation-based velocities and the remainder use observed velocities extrapolated along modelled flowlines. Our combined velocity grid is shown in Extended Data Fig. 7.

Ice masking. The task of converting line-segment observations of terminus positions into gridded ice masks is trivial to perform manually for a small set of observations but is challenging to automate for a large number of terminus positions. Extended Data Fig. 8 illustrates two initial challenges. First, a given terminus-position observation may be saved in a shapefile as several line segments that may or may not appear in order from one side of a glacier to the other. As a result, it is not possible to simply polygonize the raw shapefile data. Second, without any other context, it is not possible to automatically determine whether any given pixel in an ice mask lies upstream or downstream of a line segment that defines the terminus. So rather than treating each terminus position as part of a polygon that can be closed, we use the psnpath function in Antarctic Mapping Tools for MATLAB[54] to densify each line segment within each terminus-position observation to a spacing of 24 m along-path. In all of the remaining steps of our method, the densified terminus-position data are treated as unconnected, scattered data points rather than connected line segments.

We begin masking in the month of August 2015, using as an initial reference GimpOceanMask_90m_2015_v1.2.tif (ref. 73), which is a mosaic mask with a mean date corresponding to August 2015. Any densified terminus-position data, from any of the contributing terminus-position datasets, collected within 30 days before 15 August 2015 are then synthetically advected downstream using our velocity grid, to the expected terminus positions on 15 August 2015 assuming constant velocity and no calving. Whether or not calving occurs between the

observation date and 15 August 2015, we can be certain that any pixels downstream of the advected terminus positions can be deemed false in ice mask. Similarly, terminus positions observed within 30 days after 15 August 2015 are synthetically advected upstream to their expected location on 15 August 2015, and all pixels upstream of the advected locations can be deemed true in the ice mask on that date. We use the MATLAB stream2 function to calculate flowlines upstream and downstream of the advected terminus positions, then grid the flowline data with the gridbin function from the Climate Data Toolbox for MATLAB[74], then use imfill to fill any remaining holes in the regions that we 'carve' or 'fill' the ice mask for any given month. An illustration of carving and filling the ice mask from advected terminus-position data is provided in Extended Data Fig. 9.

From 15 August 2015, we work backward, one month at a time. We use the August mask as the initial guess for July and then update it following the method described above, using any data collected within 30 days of 15 July 2015. We continue adjusting the mask with the data of each month until 15 September 1972. Then we move forward from August 2015, following the same method until 15 February 2022. At this stage, the large-scale, secular changes in ice-sheet extent that have occurred since the 1970s are well represented in our ice mask, but further refinements are necessary to pinpoint the timing of calving events and capture the growth that can occur between observations.

We begin refining our time-evolving ice mask, starting on 15 January 2022, and using one month of displacement to interpolate the 15 February 2022 mask. Any pixels in the January mask that will flow to 'ice' (true) locations by February are overwritten as true in the January mask, because the ice in February must have flowed from a location of ice in January. However, we then repeat the method of using observations taken within 30 days of 15 January to overwrite any of these previous estimates wherever direct observations are available. Month by month, we repeat this method from 2022 to 1972. We then move forward from 1972 to 2022 using a similar philosophy, but this time adjusting the mask of each month by setting false any pixels that advected from locations that were open ocean in the previous month, before we once again overwrite with any available observations that may be directly available that month.

After two full passes forward and backward through all 594 months of the time series, the resulting time-evolving ice masks directly agree with the available observations and growth rates are physically bounded to our velocity grid and seem natural over months-long stretches in which direct observations are unavailable. However, by informing the mask of each month with past and future observations of terminus position, we introduce the possibility that the effects of a single observation error can propagate through the mask for months or years. In particular, we find that AutoTerm picks occasionally contain blunders in which the algorithm locked onto artefacts such as surface features in the ice, and some of the manually defined observations in TermPicks appear as straight lines that cut across fjords in unnatural patterns. We therefore repeat the above process, adjusting the ice mask only where several terminus-position datasets agree that a given pixel is ice or not ice. Our final, time-evolving ice mask represents a consortium of the contributing datasets, combined with a simple flow model in such a way that the mask follows the laws of physics to agree with observations while excluding outliers. We note that our model effectively interpolates terminus positions between observations but never extrapolates. Accordingly, variability on any timescale cannot be over-represented in the final data product, but some variability that occurred between observations may not be fully captured. The seasonal maximum and minimum extents, as well as long-term changes in area and mass that we report, are the result of observed changes in ice-front position and are not influenced by the velocity model. Velocity errors exceeding the width of one grid cell per month (1,440 m year^{-1}) could produce ice masking errors of one grid cell width for each month between observations and manifest as a concave or convex growth rate between dates of terminus-position observations, but velocity errors are generally well below this threshold and we do not see evidence of this issue in the data.

Ice thickness. Estimating the mass of ice lost since 1985 requires an estimate of ice thickness wherever the areal extent of the ice sheet has changed. Our ice-thickness grid is based primarily on BedMachine Greenland Version 5 (refs. 75,76). Where the ice sheet has retreated since the beginning of our observation period, BedMachine often shows zero ice thickness. In these locations, we apply a hydrostatic inversion to the surface of the AERODEM[77] elevations relative to the geoid, assuming an ice density of 917 kg m^{-3} and seawater density of 1,027 kg m^{-3}. In locations in which inversion of the AERODEM surface produces an ice base that falls below the BedMachine bed, we set ice thickness to the AERODEM surface elevation minus the BedMachine bed elevation.

Most areas of ice-sheet change are represented by finite values of ice thickness in BedMachine or AERODEM, but to create a complete ice-thickness grid that spans the entire domain around Greenland, we fill any remaining grid cells with estimates of ice thickness, which we obtain from bed-elevation values in BedMachine. We find that, along the perimeter of the ice sheet as it is defined in BedMachine, the ice is—on average—about 5% thicker than the minimum necessary to remain grounded on the bed elevations provided in BedMachine. In other words, along the perimeter of the ice sheet, at which calving occurs, an estimate of ice thickness can be obtained by multiplying the bed elevation by −1.17, which corresponds to a hydrostatic inversion plus an extra 5% thickness to keep the ice grounded. For the purposes of estimating ice-mass loss where no direct observations of past ice thickness are available, we assume that this relationship holds. Among 442,769 grid cells that experienced any change in our ice mask throughout the entire observation period, 223,785 of the grid cells contain non-zero thickness values in BedMachine, we use 129,229 thickness estimates from AERODEM and the remaining 89,729 thickness values are estimated by assuming that the ice is −1.17 times the elevation value in BedMachine. Our combined ice-thickness grid is shown in Extended Data Fig. 7.

Thickness-error estimates are taken as the formal estimates provided with the BedMachine product for any grid cells that use BedMachine thickness data. For AERODEM, we assume 10 m surface elevation error, which translates to 93.4 m thickness error where the ice is assumed to have been floating hydrostatically (Archimedes' principle). Where the ice was grounded, the AERODEM thickness uncertainty is estimated as the root sum square of 10 m surface elevation error and the BedMachine bed elevation error. We find that, along the perimeter of the ice sheet, our model of ice-thickness estimate from bed elevations matches BedMachine thickness values with a standard deviation of 32.7 m. Where we use bed elevation to estimate ice thickness, we assume that the thickness error is the root sum square of 1.17 times the bed error estimates and 32.7 m. Bed elevation error estimates are shown in Extended Data Fig. 10. Note that our method of mosaicking several observational products to estimate ice thickness can result in apparent discontinuities in ice thickness at boundaries of contributing datasets, but our uncertainty estimates capture this effect accordingly.

Glacier catchments. We use 260 named Glacier catchments for the GrIS[78]. To account for terminus activity that may have occurred beyond the extents of the predefined glacier catchments, we extrapolate each catchment downstream following flowlines from our velocity grid. Each catchment is then dilated by 5 km to fill any gaps between extrapolated flowlines and fjord walls or neighbouring catchments. Our extrapolated catchment delineations are shown in Extended Data Fig. 11.

Ice-sheet area and mass time series. The area of each glacier catchment is calculated by summing the area of all ice grid cells within each glacier catchment, for each monthly time step. Polar stereographic distortion is accounted for using the psndistortion function in Antarctic Mapping Tools for MATLAB[54]. For each catchment, we estimate error as

the sum of the area of all grid cells within a 1-pixel perimeter along the edge of the ice sheet. This assumes that terminus-position errors are fully correlated within each glacier catchment. When calculating the total area of the entire ice sheet, we assume that errors are uncorrelated between catchments and, therefore, estimate the ice-sheet-wide area error as the root sum square of the 260 catchment errors.

The mass of ice in each glacier catchment is calculated as the sum of the product of the area, thickness and ice density (917 kg m^{-3}) of all ice grid cells within each catchment. Mass errors arise primarily from thickness error and terminus-position error. Mass errors owing to thickness uncertainty are described above and mass associated with terminus-position error is calculated as the sum of the mass of all grid cells within a 1-pixel perimeter along the edge of the ice sheet. We estimate the error of the mass measurement within each glacier catchment as the root sum square of thickness and terminus-position errors. Following the method used for estimating the area error for the entire ice sheet, we assume that errors are uncorrelated between catchments and estimate the total mass error as the root sum square of the 260 catchment errors. Note that our velocity grid is primarily used to limit the rate of ice-front advance between months of observation, meaning that velocity errors would need to exceed 120 m per month to result in a 1-pixel-width area error, which corresponds to our estimates of area error for any given month and any given glacier. Our approach to measuring velocity uncertainty and its impacts on area and mass uncertainty is heuristic, but the signals of area change that we measure are large enough that any reasonable approach to uncertainty quantification would yield uncertainty estimates orders of magnitude smaller than the signals of change.

Correlation analysis. Terminus thickness and width are defined using the mean thickness and total number of ocean-adjacent ice-sheet perimeter pixels within each catchment, taken from the most retreated position of the ice sheet. Surface slope and bed slope are calculated by fitting trend lines to topography along flow paths from each perimeter grid cell of the ice sheet to 5 km upstream and a single slope value is assigned to each catchment as the thickness-weighted mean of the slopes calculated from each grid cell. The terminus velocity of each glacier is taken as the mean velocity of the ice-sheet perimeter pixels within each catchment. Steady-state ice flux is calculated for each catchment using a method that we have previously applied to Antarctica[79]. Surface runoff is summed for each catchment using GSFC-FDMv1.2.1 (ref. 80), from the gridded mean of all runoff from the years 2000–2020, converted to units of Gt $year^{-1}$. Runoff values are normalized by glacier catchment area when comparing with glacier equivalent length values. Sill depth is calculated with a digital elevation model of bed elevations from BedMachine plus our ice-thickness values wherever ice is always observed. We use the fillsinks function in TopoToolbox[81] to fill the digital elevation model to the height of local sill depths within fjords. Ocean temperatures are compiled from 2,828 oceanographic profiles collected by NASA's Oceans Melting Greenland campaign[82–84] from 2015 to 2022 (Extended Data Fig. 5). We subtract the mean temperature profile from all 2,828 observations to obtain a profile of temperature anomalies for each location and then calculate a mean anomaly temperature in the top 1,000 m of each profile to obtain a scalar mean temperature anomaly for each of the 2,828 profile locations. By removing the overall mean vertical profile from each individual profile, we are better able to compare the spatial distribution of temperatures among profiles that may reach different depths. For each catchment, we then calculate the mean of all mean anomaly temperatures within 10 km of each glacier terminus. We experimented with a range of distance-to-glacier thresholds and found no meaningful difference in any of our results when using a 1-km threshold or a 10-km threshold, so we use 10 km to maximize the number of glaciers (95) that could be directly compared with the available data in Fig. 4 and Extended Data Fig. 4.

Mass and area change calculations. Long-term 'secular' changes in mass and area are calculated as the difference between values corresponding to February 1985 and February 2022 in a 12-month moving mean of each time series. Secular change error is estimated as the root sum square of uncertainties of the 1985 and 2022 measurements. Twenty-first century trends are calculated by least-squares-fit monthly measurements from January 2000 to February 2022.

Data availability

The monthly ice masks described in this work were developed for the NASA MEaSUREs ITS_LIVE project and are available through the National Snow and Ice Data Center at https://doi.org/10.5067/579TO87M7IZB.

Code availability

An archived version of the code used to create the monthly ice masks, analyse the data and create the figures in this manuscript is available at https://doi.org/10.5281/zenodo.8388136. Any updates to the code will be available at https://github.com/chadagreene/greenland-icemask.

55. Zhang, E., Catania, G. & Trugman, D. AutoTerm: a "big data" repository of Greenland glacier termini delineated using deep learning. https://egusphere.copernicus.org/preprints/2022/egusphere-2022-1095/ (2022).
56. Enze, Z. AutoTerm: a "big data" repository of glacier termini delineated using deep learning. *Zenodo* https://doi.org/10.5281/ZENODO.7782039 (2022).
57. Black, T. MEaSUREs weekly to monthly Greenland outlet glacier terminus positions from Sentinel-1 mosaics, version 1. *National Snow and Ice Data Center (NSIDC)* https://doi.org/10.5067/DGBOSSIULSTD (2022).
58. Joughin, I. & University Of Washington. MEaSUREs annual Greenland outlet glacier terminus positions from SAR mosaics, version 2. *National Snow and Ice Data Center (NSIDC)* https://doi.org/10.5067/ESFWE11AVFKW (2021).
59. Cheng, D. et al. Calving Front Machine (CALFIN): glacial termini dataset and automated deep learning extraction method for Greenland, 1972–2019. *Cryosphere* **15**, 1663–1675 (2021).
60. Cheng, D., Hayes, W. & Larour, E. CALFIN subseasonal Greenland glacial terminus positions, version 1. *National Snow and Ice Data Center (NSIDC)* https://doi.org/10.5067/7FILV218JZA2 (2021).
61. Goliber, S. et al. TermPicks: a century of Greenland glacier terminus data for use in scientific and machine learning applications. *Cryosphere* **16**, 3215–3233 (2022).
62. Goliber, S. & Black, T. TermPicks: a century of Greenland glacier terminus data for use inmachine learning applications. *Zenodo* https://doi.org/10.5281/ZENODO.5117931 (2021).
63. Gardner, A., Fahnestock, M. & Scambos, T. MEaSUREs ITS_LIVE regional glacier and ice sheet surface velocities, version 1. *National Snow and Ice Data Center (NSIDC)* https://doi.org/10.5067/6II6VW8LLWJ7 (2022).
64. Gardner, A. S. et al. Increased West Antarctic and unchanged East Antarctic ice discharge over the last 7 years. *Cryosphere* **12**, 521–547 (2018).
65. Joughin, I. MEaSUREs Greenland ice velocity annual mosaics from SAR and Landsat, version 1. *National Snow and Ice Data Center (NSIDC)* https://doi.org/10.5067/OBXCG75U7540 (2017).
66. Larour, E., Seroussi, H., Morlighem, M. & Rignot, E. Continental scale, high order, high spatial resolution, ice sheet modeling using the Ice Sheet System Model (ISSM). *J. Geophys. Res. Earth Surf.* **117**, F01022 (2012).
67. Briner, J. P. et al. Rate of mass loss from the Greenland Ice Sheet will exceed Holocene values this century. *Nature* **586**, 70–74 (2020).
68. Cuzzone, J. K. et al. The impact of model resolution on the simulated Holocene retreat of the southwestern Greenland ice sheet using the Ice Sheet System Model (ISSM). *Cryosphere* **13**, 879–893 (2019).
69. Cuzzone, J. K., Young, N. E., Morlighem, M., Briner, J. P. & Schlegel, N.-J. Simulating the Holocene deglaciation across a marine-terminating portion of southwestern Greenland in response to marine and atmospheric forcings. *Cryosphere* **16**, 2355–2372 (2022).
70. Goelzer, H. et al. The future sea-level contribution of the Greenland ice sheet: a multi-model ensemble study of ISMIP6. *Cryosphere* **14**, 3071–3096 (2020).
71. Dias Dos Santos, T., Morlighem, M. & Brinkerhoff, D. A new vertically integrated MOno-Layer Higher-Order (MOLHO) ice flow model. *Cryosphere* **16**, 179–195 (2022).
72. Cuzzone, J. K., Morlighem, M., Larour, E., Schlegel, N. & Seroussi, H. Implementation of higher-order vertical finite elements in ISSM v4.13 for improved ice sheet flow modeling over paleoclimate timescales. *Geosci. Model Dev.* **11**, 1683–1694 (2018).
73. Howat, I., Ohio State University & Byrd Polar Research Center. MEaSUREs Greenland Ice Mapping Project (GIMP) land ice and ocean classification mask, version 1. *National Snow and Ice Data Center (NSIDC)* https://doi.org/10.5067/B8X58MQBFUPA (2017).
74. Greene, C. A. et al. The Climate Data Toolbox for MATLAB. *Geochem. Geophys. Geosyst.* **20**, 3774–3781 (2019).
75. Morlighem, M. et al. BedMachine v3: complete bed topography and ocean bathymetry mapping of Greenland from multibeam echo sounding combined with mass conservation. *Geophys. Res. Lett.* **44**, 11,051–11,061 (2017).
76. Morlighem, M. IceBridge BedMachine Greenland, version 5. *National Snow and Ice Data Center (NSIDC)* https://doi.org/10.5067/GMEVBWFLWA7X (2022).
77. Korsgaard, N. J. et al. Digital elevation model and orthophotographs of Greenland based on aerial photographs from 1978–1987. *Sci. Data* **3**, 160032 (2016).

78. Mouginot, J. & Rignot, E. Glacier catchments/basins for the Greenland Ice Sheet. *Dryad* https://doi.org/10.7280/D1WT11 (2019).
79. Greene, C. A., Gardner, A. S., Schlegel, N.-J. & Fraser, A. D. Antarctic calving loss rivals ice-shelf thinning. *Nature* **609**, 948–953 (2022).
80. Medley, B., Neumann, T. A., Zwally, H. J. & Smith, B. E. Forty-year simulations of firn processes over the Greenland and Antarctic ice sheets. https://tc.copernicus.org/preprints/tc-2020-266/tc-2020-266.pdf (2020).
81. Schwanghart, W. & Scherler, D. Short Communication: TopoToolbox 2 – MATLAB-based software for topographic analysis and modeling in Earth surface sciences. *Earth Surf. Dyn.* **2**, 1–7 (2014).
82. Oceans Melting Greenland (OMG). OMG CTD Conductivity Temperature Depth (CTD) profiles. Jet Propulsion Laboratory https://doi.org/10.5067/OMGEV-CTDS1 (2020).
83. Fenty, I. et al. Oceans Melting Greenland: early results from NASA's ocean-ice mission in Greenland. *Oceanography* **29**, 72–83 (2016).
84. Willis, J. et al. Ocean-ice interactions in Inglefield Gulf: early results from NASA's Oceans Melting Greenland mission. *Oceanography* **31**, 100–108 (2018).

Acknowledgements We thank T. Black, D. Cheng, S. Goliber, I. Joughin and E. Zhang for making their terminus-position data available to the public and for many helpful discussions about their data. This research was supported by the NASA Cryospheric Science and MEaSUREs programmes and was conducted at the Jet Propulsion Laboratory, California Institute of Technology, under contract with the National Aeronautics and Space Administration ©2023. All rights reserved.

Author contributions C.A.G. and A.S.G. conceived the study. C.A.G. generated the ice masks, analysed the ice time series data, created all figures and wrote the first draft of the manuscript. M.W. provided oceanographic data and assisted in the oceanographic data analysis. J.K.C. provided ice-sheet-model data and assisted in their application to this work. All authors contributed to revisions and the final draft of this manuscript.

Competing interests The authors declare no competing interests.

Additional information
Supplementary information The online version contains supplementary material available at https://doi.org/10.1038/s41586-023-06863-2.
Correspondence and requests for materials should be addressed to Chad A. Greene.
Peer review information *Nature* thanks Vincent Verjans and the other, anonymous, reviewer(s) for their contribution to the peer review of this work. Peer reviewer reports are available.

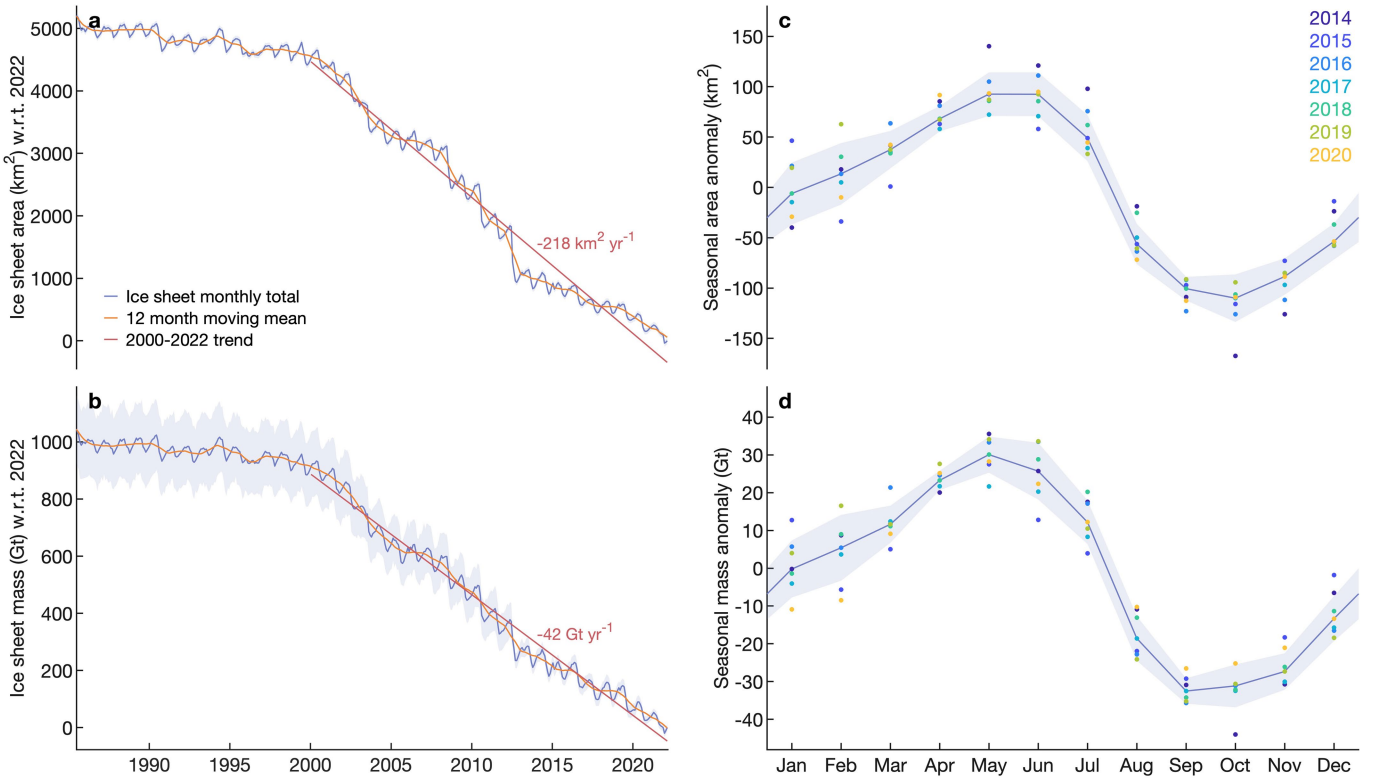

Extended Data Fig. 1 | GrIS area and mass variability. Pan-Greenland totals show that the ice sheet has lost 5,091 ± 72 km^2 of its area (**a**) or 1,034 ± 120 Gt of mass (**b**) to glacier terminus retreat since 1985. Seasonal cycles of area (**c**) and mass (**d**) are characterized by the median of residuals for the years 2014–2020, after subtracting a 12-month moving average from the full monthly time series. Shaded blue regions in all panels indicate measurement uncertainty, estimated from the root sum square of uncertainties related to terminus position and ice thickness for each glacier (Methods).

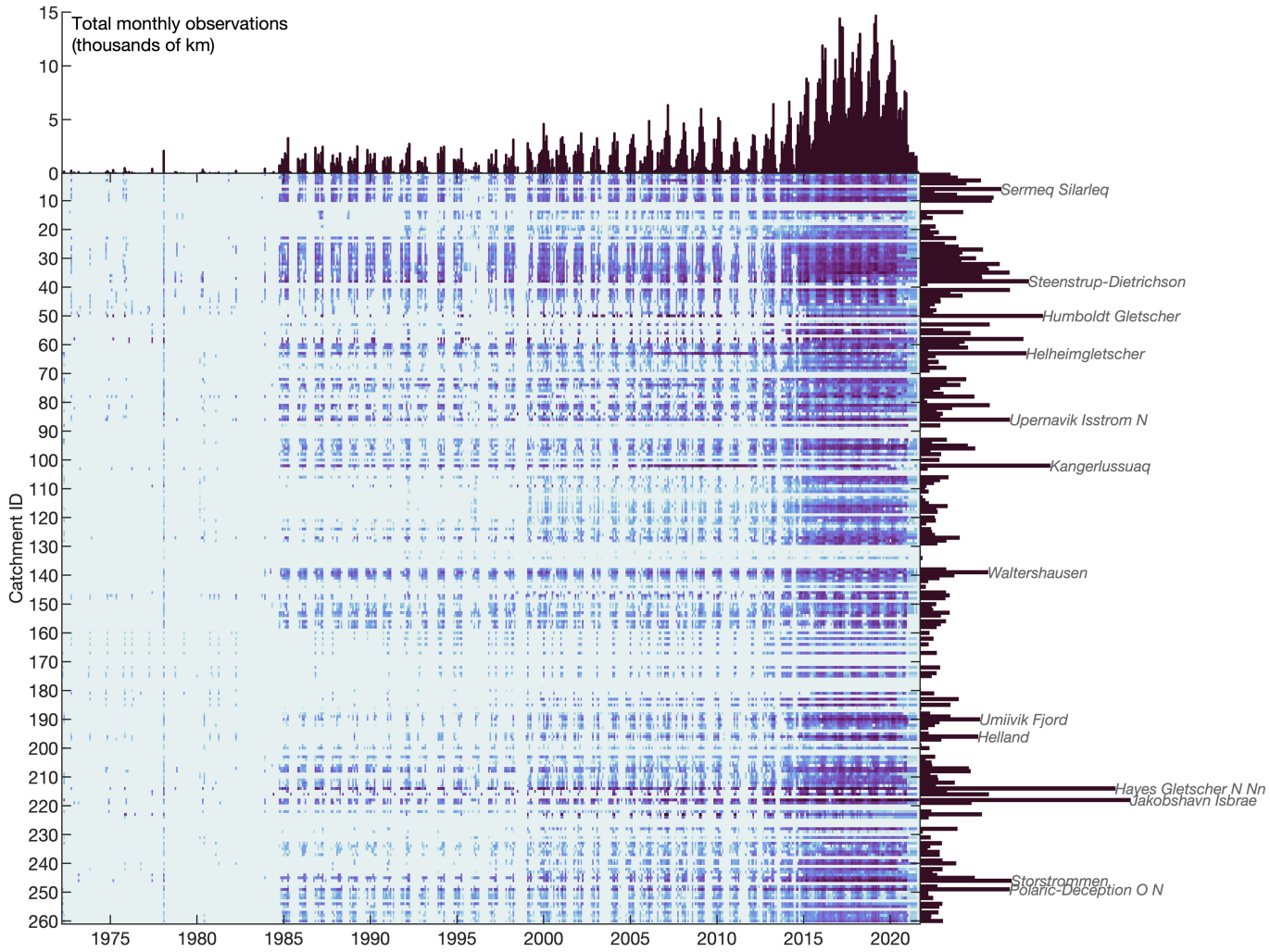

Extended Data Fig. 2 | Observation data density. The total length of terminus observation data within each glacier catchment is summed for each month of the time series, as a proxy for which glaciers are best observed and when. Colour is presented on a log scale, in which dark purple indicates a high density of data. Histograms along the top and side of the matrix show totals, indicating when observations are available and which glaciers are best sampled. We use data collected as early as 1972 to constrain our ice masks, but the data analysis presented in this paper begins in 1985.

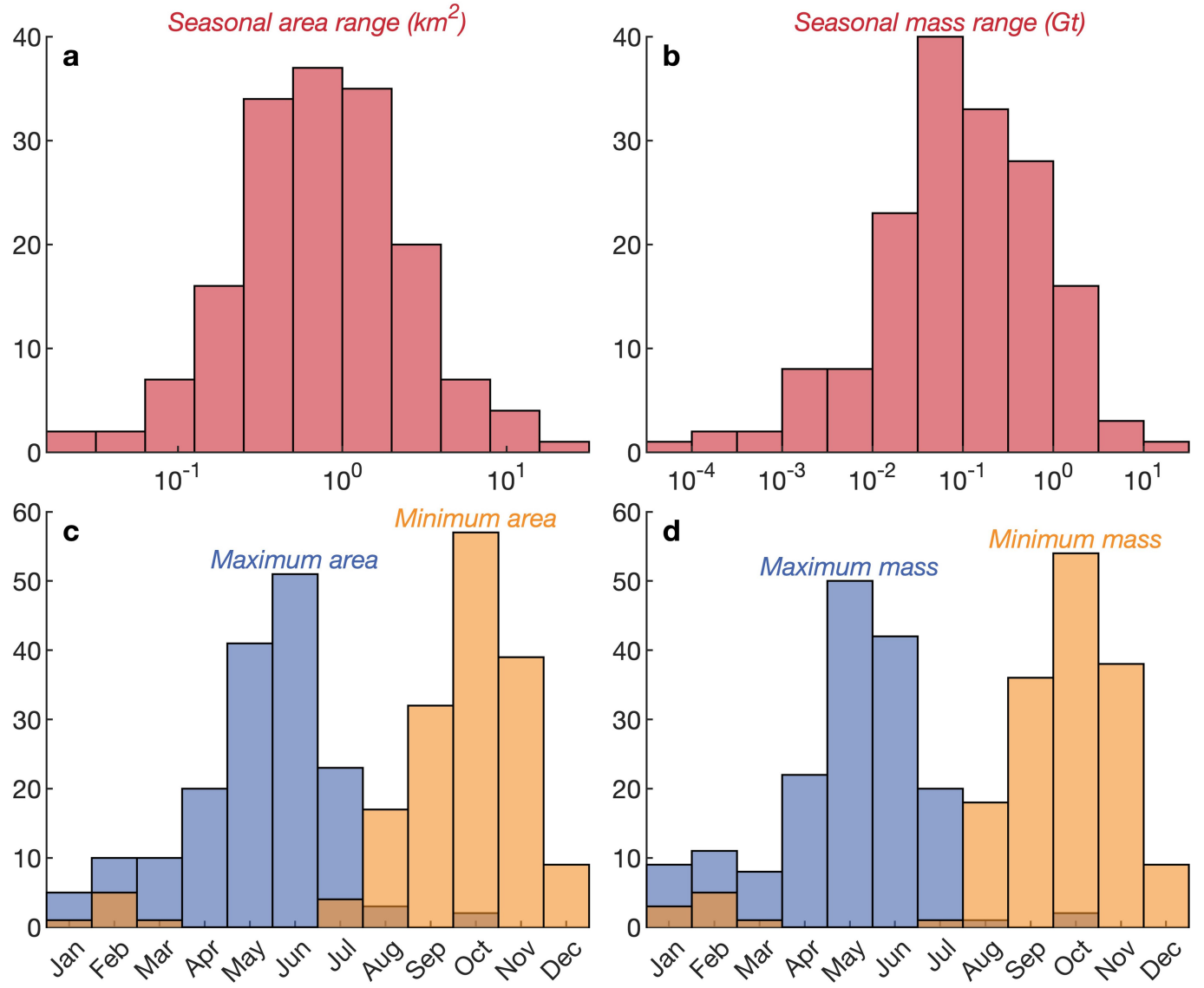

Extended Data Fig. 3 | Distributions of seasonal amplitudes and phases. 178 marine-terminating glaciers in Greenland exhibit substantial, consistent seasonal variability in terminus position each year. The median range of minimum-to-maximum glacier extent within a given year is about 0.8 km^2 (**a**) or 0.1 Gt (**b**) per glacier, but glacier sizes roughly follow a Pareto distribution, meaning that a few glaciers have seasonal ranges that are 10 to 20 times larger than the GIS median. Glaciers tend to reach their maximum area (**c**) and mass (**d**) in May or June, then retreat to a minimum that occurs around October. Most glaciers exhibit a maximum and minimum extent that occurs slightly after the overall ice-sheet average, largely because of the influence that the early cycle of Jakobshavn Isbræ has on the areal extents and total mass of the entire ice sheet.

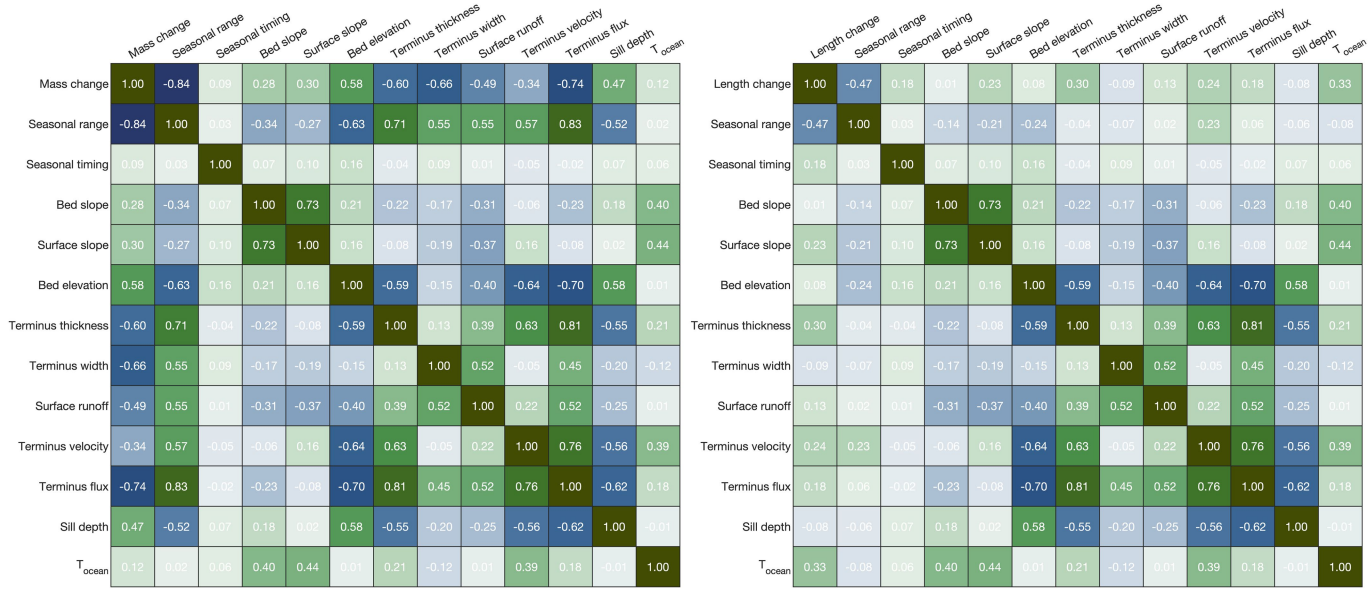

Extended Data Fig. 4 | Correlations between retreat and local environmental factors. A matrix of correlation coefficients (*r*) compares relationships between glacier mass change owing to calving, the range of seasonal mass variability owing to calving, the timing of seasonal maximum mass, bed slope and surface slope within 5 km of the glacier terminus, bed elevation, thickness, velocity and ice flux at the terminus, mean surface runoff from each catchment, oceanographic sill depth and mean ocean-temperature anomalies measured within 10 km of each glacier terminus, compared for 95 glaciers for which observations of all variables are available. The top row of the mass variability correlation matrix distils the results shown in Fig. 4, and negative values indicate that glaciers tend to lose mass where the dependent variable is higher. To account for relationships between mass and glacier terminus thickness and width, we normalize mass values by glacier terminus face area, providing a measure of effective length variability that reveals that seasonal variability is the strongest simple predictor of long-term retreat.

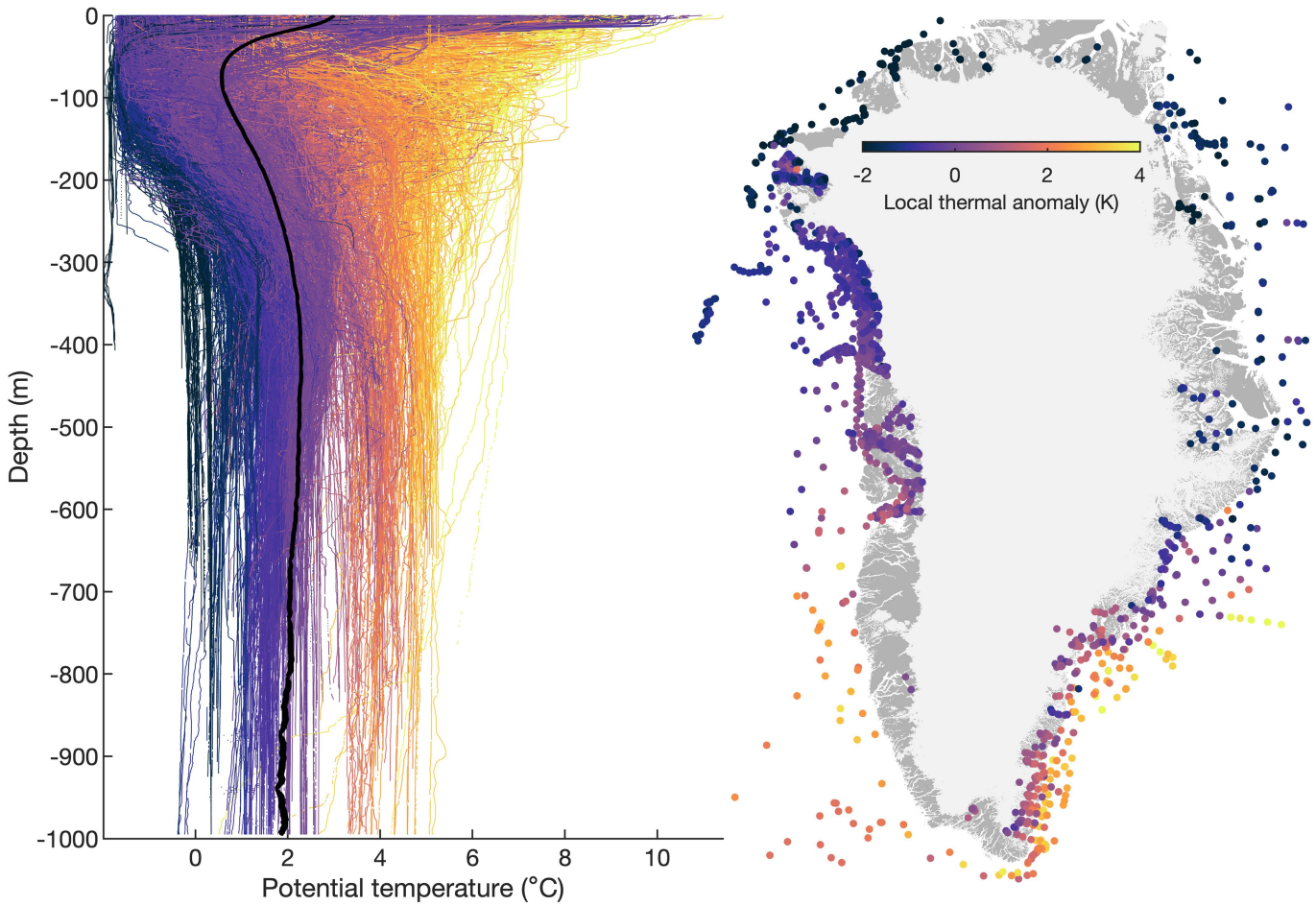

Extended Data Fig. 5 | Ocean-temperature observations. We use 2,828 oceanographic temperature profiles collected by NASA's Oceans Melting Greenland project. Each profile on the left is colour-scaled by a scalar local thermal anomaly value shown in the map on the right. The heavy black profile on the left represents the mean of all 2,828 profiles. By subtracting the mean profile from each individual profile and then calculating a mean anomaly value within the top 1,000 m of each profile, we obtain a measure of ocean temperature that reflects the spatial distribution of available heat energy, with minimal influence from the depth of the available observations. Map created with Arctic Mapping Tools for MATLAB[54] using geographic outlines developed in this work.

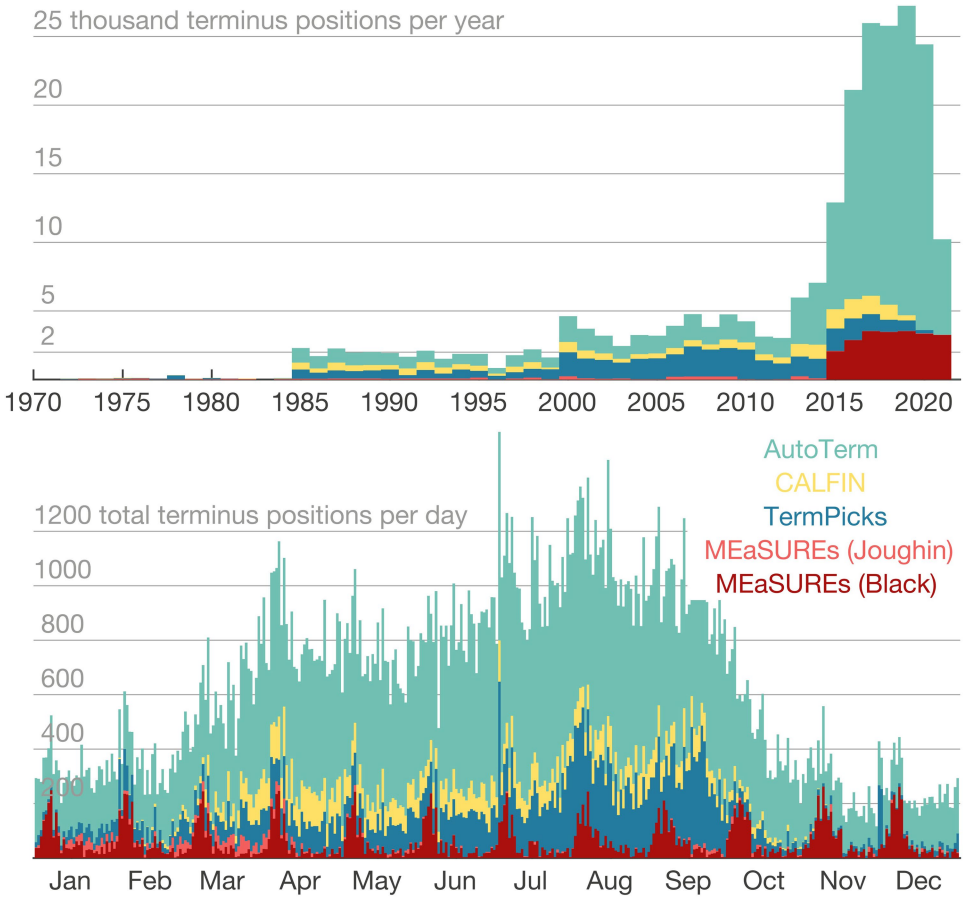

Extended Data Fig. 6 | Terminus observation timing by dataset. We use terminus-position observations from five sources (Methods) to analyse changes in the extent of the GrIS since 1985 and we use observations from 2014 to 2020 to characterize the seasonal cycles of growth and retreat of the ice sheet.

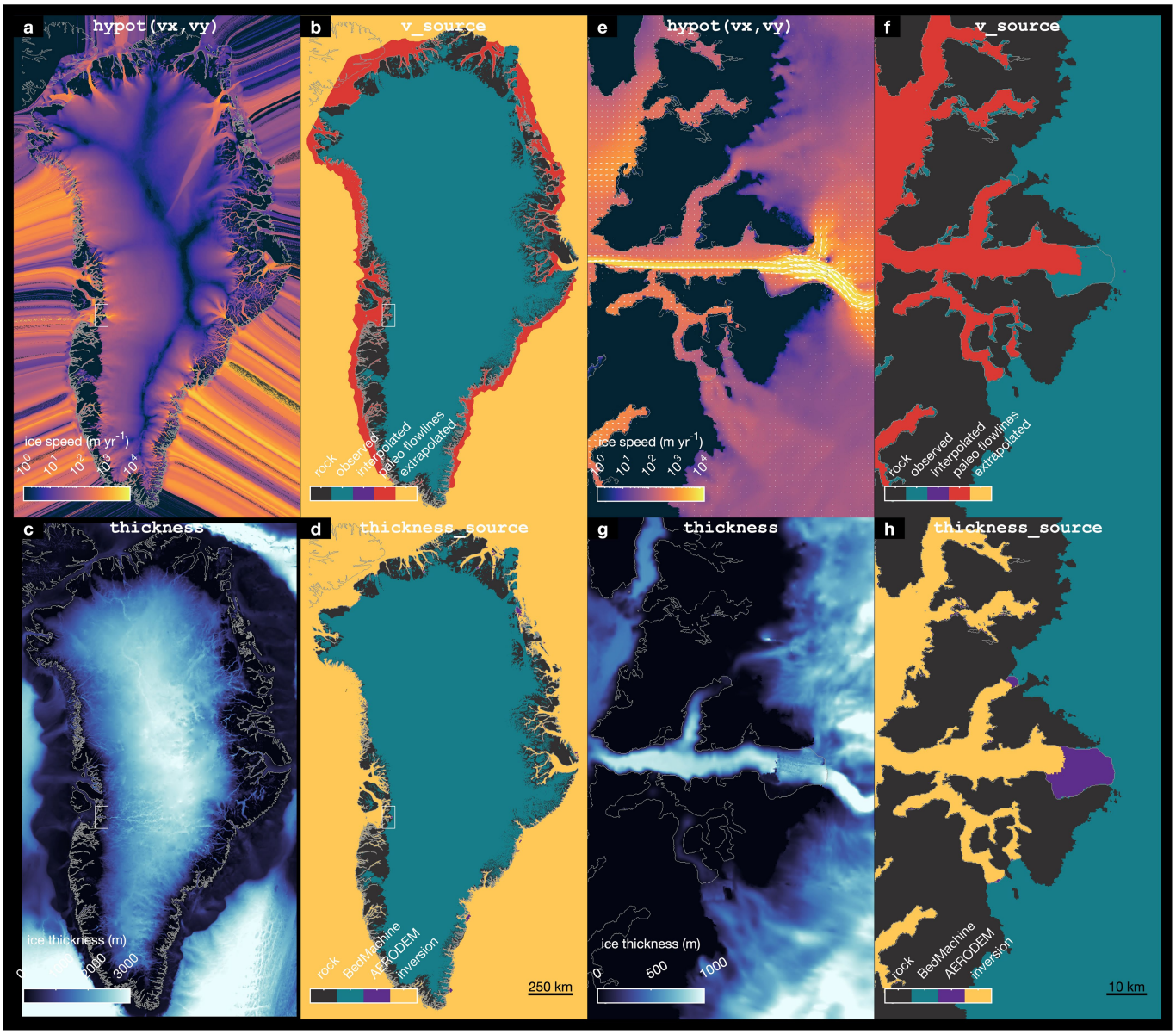

Extended Data Fig. 7 | Gridded velocity and thickness data. This work required knowledge of ice velocity and thickness beyond the current measurable extents of the ice sheet. We combine data from several sources (Methods) to generate complete gridded velocity and thickness fields that cover the entire domain of interest. Ice velocity and thickness values are unrealistic in the open ocean but are reasonable and well constrained within fjords and close to the current extents of the ice sheet, for which the values are used in this work. **a**–**d**, The entire GrIS. **e**–**h**, Detailed views of the region surrounding the terminus of Jakobshavn Isbræ. Maps created with Arctic Mapping Tools for MATLAB[54] using geographic outlines developed in this work.

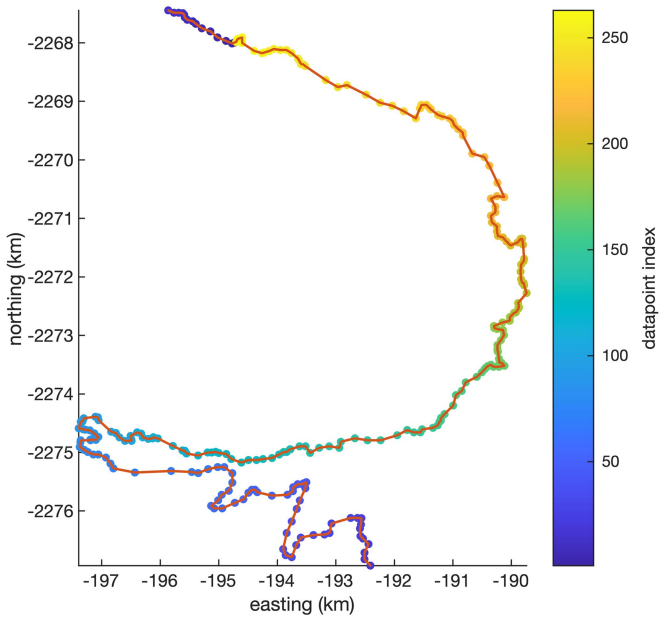

Extended Data Fig. 8 | Terminus-position data densification. An example of the terminus-position data we use is shown as 260 blue-to-yellow coloured dots. Raw terminus-position data are not necessarily distributed as continuous line segments from one side of a glacier terminus to the other, as seen by the blue dots that start near the top and then continue at the bottom of the image above. We sort and densify all terminus-position data and then use a flow model to determine whether any given point lies upstream or downstream of the observed terminus position (Methods). Map created with Arctic Mapping Tools for MATLAB[54] with terminus position from the TermPicks dataset[61].

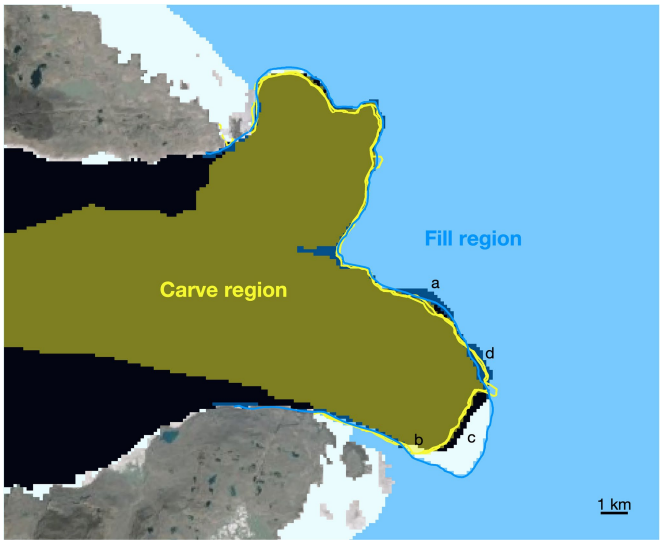

Extended Data Fig. 9 | Masking process example. An ice mask representing a previous assumption (Methods) is shown in white. Blue lines show all terminus observations taken within 30 days after 15 August 2015 and advected upstream to their expected location on 15 August 2015. Yellow lines show terminus observations taken within 30 days before 15 August 2015 and advected downstream to their expected location on 15 August 2015. **a**, All pixels upstream of the blue lines are in the 'Fill region' and are set as true in the ice mask. **b**, Pixels downstream of the yellow line defined as being in the 'Carve region' and are set as false in the ice mask. **c**, No adjustments are made where the Prior mask terminus falls between the Carve region and the Fill region. This can occur when ice is lost to calving in the time between terminus observations or it can be because of a mismatch in terminus-position picks. **d**, We set ice pixels to true wherever downstream-advected and upstream-advected terminus positions overlap. Map created with Arctic Mapping Tools for MATLAB[54] using geographic outlines developed in this work.

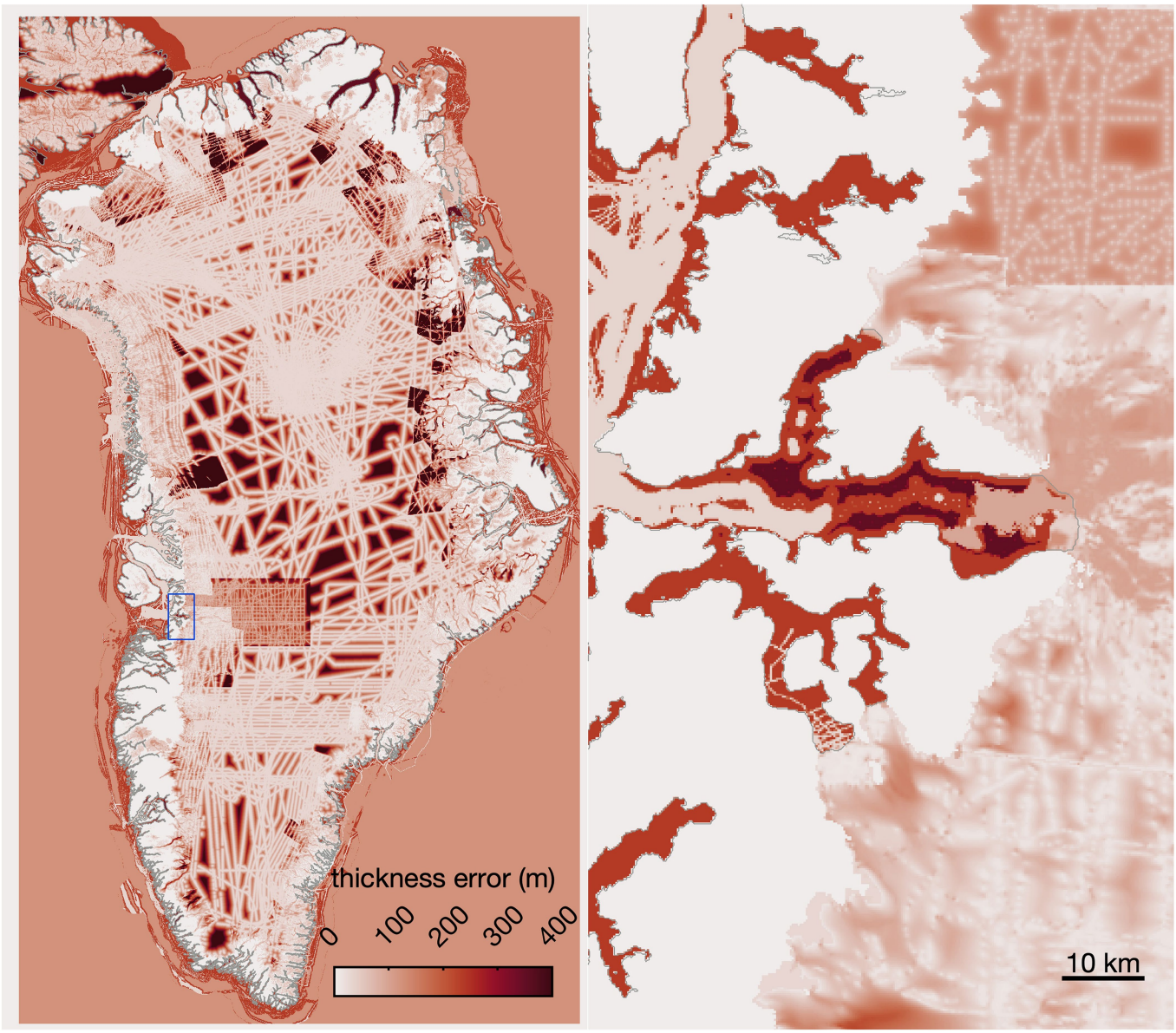

Extended Data Fig. 10 | Ice-thickness uncertainty. Errors in ice thickness are estimated on the basis of the source of the thickness data (Methods). The inset in the right panel matches the inset in Extended Data Fig. 7. Maps created with Arctic Mapping Tools for MATLAB[54] using geographic outlines developed in this work.

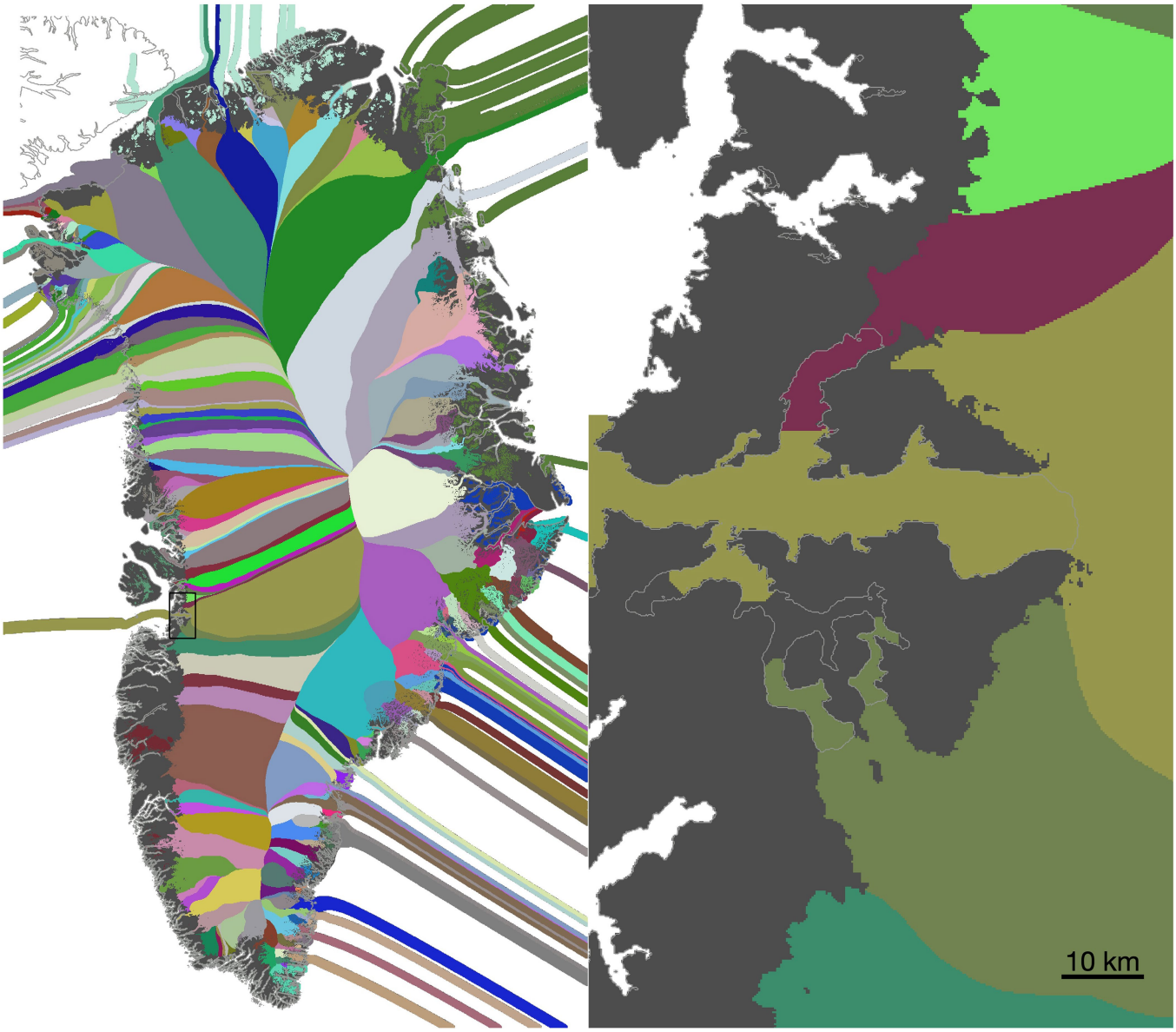

Extended Data Fig. 11 | Extrapolated glacier catchments. To properly account for terminus activity that occurred beyond the present-day extents of the ice sheet, we extrapolate 260 glacier catchment regions downstream along our extrapolated flowlines (Extended Data Fig. 7) and then dilate each catchment area by up to 5 km to fill any gaps near fjord walls. The inset in the right panel matches the inset in Extended Data Fig. 7. Maps created with Arctic Mapping Tools for MATLAB[54] using geographic outlines developed in this work.